Imaging the mouse lung with micro-CT

Wolfgang Recheis, Ann V. Clough, Steven T. Haworth, Geoffrey McLennan,
Alan F. Ross, and Eric A. Hoffman

Corresponding author: Eric A Hoffman

Wolfgang Recheis, PhD
University of Iowa, Carver College of Medicine
Division of Physiologic Imaging, Department of Radiology
200 Hawkins Drive
52242 Iowa City
wolfgang-recheis@uiowa.edu

Geoffrey McLennan, MD., PhD.,
Professor of Medicine and Biomedical Engineering
Department of Medicine, Division of Pulmonary Diseases
University of Iowa, Carver College of Medicine
200 Hawkins Drive
52242 Iowa City
Geoffrey-mclennan@uiowa.edu

Ann V Clough, PhD, Professor of Mathematics
Department of Mathematics, Statistics and Computer Science
Marquette University
PO Box 1881
Milwaukee, WI 53201-1881
ann.clough@marquette.edu

Alan F Ross, MD, Associate Professor
Department of Anesthesia,
University of Iowa, Carver College of Medicine
200 Hawkins Drive
52242 Iowa City
alan-ross@uiowa.edu

Steven T Haworth, PhD, Assistant Professor of Medicine
Division of Pulmonary and Critical Care Medicine
Medical College of Wisconsin
Research Service 151
Zablocki VA Medical Center
5000 W. National Avenue
Milwaukee, WI 53295
shaworth@mcw.edu

Eric A Hoffman, PhD, Professor of Radiology and Biomedical Engineering
University of Iowa, Carver College of Medicine
Division of Physiologic Imaging, Department
of Radiology
200 Hawkins Drive
52242 Iowa City
eric-hoffman@uiowa.edu

I. Introduction

Computed tomography (CT) of the lung has made major advances in hardware and software over the last decade. The human lung can now be imaged rapidly and volumetrically, with the digital information being easily transported, stored, reviewed, and both subjectively and objectively analyzed (1), (2). Figure 1 depicts a set of examples spanning anatomic segmentation (3), (4), (5), (6), (7), (8), automatic labeling (9), image based lung modeling (10), (11), ventilation (12), (13) and perfusion imaging (14), (15), morphometric correlation to in-vivo imaging (16), and large animal model of evolving lung inflammation. In large animal models functional imaging demonstrates the early changes in pathology (17). Our methods are demonstrating that the texture measures of both anatomic features and function provide the early signs of pathologic processes (2). Still there remains a need to correlate pathologic phenotypes with genotypes and to phenotype diversity at the alveolar/bronchiola and arteriolar levels in-vivo and in-situ.

It is our view that micro-CT will have a profound influence on the documentation of anatomical and physiological phenotypic changes in the many genetic mouse models. The mapping of the human genome, together with that of other animals and plants is providing enormous new information the signature of which will emerge fully over the next few decades. The animal model that receives wide attention for the study of genetic based diseases is the mouse. The animal is small and inexpensive to house. The genetics are well studied, and the specific genetic deficient or efficient animals can be bred for the study of hundreds of diseases. Genetically modified animals are developed to answer a specific question. Frequently, abnormalities are noted within the animals, outside of the targeted organ or the specifically biological defect induced. The full phenotype of these animals may include anatomical and physiological abnormalities, in addition to the biochemical and genetic changes. Describing these abnormalities fully is key to understanding the complex interaction of genetic influences. While individual animals are relatively inexpensive, the cost of developing a model can be very significant. This is amplified when animals must be sacrificed and studied at multiple time points during growth or at multiple time points during the development of a disease. Determination of such time points is somewhat arbitrary, and important information may not be recorded if incomplete observations are made. Micro-CT scanning will allow numerous experiments in mouse models to be planned with greater precision. The cost of exploring the complex phenotypic expression of genetic changes will be reduced and longitudinal studies will be greatly facilitated by allowing more complete and accurate description of events. As shown in Figure 2, mouse imaging via conventional CT lacks the spatial resolution needed. To maximize the potential of micro-CT to quantitatively evaluate the mouse lung, imaging protocols, reconstruction algorithms and image analysis methods all must be established and specifically tailored to in-vivo, in-situ and ex-vivo imaging of lung tissue.

The normal mouse lung differs from the human lung in lung size, reported alveolar size, lung segmentation into different lobes, and a different respiratory rate (18). A growing number of genetic mouse models are being developed specifically for studying the effects on the lung. Understanding phenotypic lung expression is key, and may be facilitated by the development of a CT derived structural lung atlas of the normal adult mouse. Such a reference image library for the mouse lung currently does not exist. Mouse models of human disease create the opportunity to evaluate structural and functional characteristics that cannot easily be assessed in the human. Mouse models of many diseases have now been developed through environmental or genetic approaches including transgenic animals. Mouse models do not always replicate human pathophysiology. For example the cystic fibrosis transgenic mouse does not develop the same type of lung disease as the human counterpart (19). There are however, reasonable mouse models of pulmonary emphysema from either smoking or various genetic abnormalities. Mouse lung disease research has been recently augmented by the development of specific mouse ventilators and pulmonary function testing equipment (18), by the coincident development of the micro-CT scanner built specifically for mouse studies, and the development of 3D microscopy/pathology techniques. These three complementary techniques will allow information rich cross-sectional and longitudinal studies in the normal animal as well as relevant environmentally-induced and genetic lung disease models.

The use of micro-CT is not only limited to small rodent imaging. There is an increased interest of studying structures in biopsy probes of humans and large animals. We are establishing the methods which will allow imaging of the respiratory system of a mouse (in-vivo, in-situ and ex-vivo) by micro CT with repeatable accuracy. The acquired spatial and density information will establish a normative atlas against which early pathologic processes can be detected and followed. The information below is a summary of that process in relation to methods of x-ray imaging in general and micro-CT specifically.

II. Technical principals and overview of micro-CT

The basic principles of micro CT or cone-beam CT have been described by a number of papers. The topics range from mathematical theories on cone beam reconstruction, or detector and x-ray source design to practical applications. Jorgensen et.al., Ritman et.al. and Rüegsegger et.al (20), (21), (22) (23) give a good overview of the technical basics of micro-CT. Micro-CT continues to advance with improving hardware and software. Recent applications of micro-CT to lung imaging in the mouse are discussed below.

A. Micro-CT introduction

Micro-CT scanners have inherent system limitations in signal-to-noise ratio (SNR) performance due to their small voxel size and relatively low x-ray exposure level, but can be effectively used to scan the bony structures of a small animal (24), (25), (26). In-vivo soft tissue imaging is still a challenge because long exposure times cause motion artifacts, which limit spatial resolution and signal-to noise ratio. The first commercially available

micro-CT devices came to market only a few years ago (27). The invention and introduction of high-resolution CCD detectors (up to 4k by 4k matrix and more) together with X-ray sources having small and variable focal spots combined with relatively high power, allow in-vivo lung scanning to be possible. Table 1 gives an overview of some commercially available systems that are designed for in-vivo studies. Note that this table is certainly not complete and only a few parameters of the various scanners are presented. Figure 3 shows two different design possibilities of micro-CT. In the upper panel (developed at the Marquette University), the system rotates the animal or specimen. In the lower panel the system rotates the x-ray tube and detector around the animal. An important trade off is the cumulative dose exposure during the scan when long term survival in-vivo studies are considered (28).

B. Micro focal sources of x-ray production

Micro-CT scanners use mostly micro-focal x-ray sources, except in very special cases where other x-ray sources are being applied such as synchrotron radiation, laser induced x-ray production or conventional x-ray tubes (29), (30).

The focal spot is the region of an X-ray tube anode from which the x-rays emanate as a result of electron impact. The size of the focal spot is a critical parameter in many x-ray imaging systems, including projection radiography and computed tomography, and certainly micro-CT. New generations of x-ray tubes for cone beam micro-CT have a focal spot size of below 1 μm. A smaller focal spot size generally allows for better resolution. This effect, sometimes called geometric unsharpness, depends up on the location of the object in the source-to-detector direction. The resolution impact of the focal spot increases with geometric magnification, i.e. increasing distance between the object and the detector for a fixed source-to-detector distance. Thus, a small focal spot is desired in order to optimize spatial resolution.

The power of micro focal x-ray tubes range between 4 and 100 Watts. X-ray tubes above 10-20 Watts need to have a variable focal spot to prevent the (tungsten) anode from melting or evaporating, because the electron impact for x-ray production is focused on the small focal area. Therefore if an x-ray tube is operating at its power limit, decreasing the size of the focal spot will require a decrease in the tube current. There is, therefore, a trade-off between increased spatial resolution due to the smaller size of the focal spot, and increased image noise in a fixed exposure time due to the necessary decrease in x-ray intensity.

C. Filters

Commercially available micro-CT systems utilize x-ray sources with tungsten as anode material which has a characteristic x-ray emission spectrum. This spectrum has a significant peak at about 60kV and a second peak at 67 kV at a typical maximum kinetic

energy of the electrons of 100kV (Figure 4). It is known that tissue absorbs x-rays better with lower energy photons (about energy-^{3} dependence in regions below 25 kV) (31).

There are attempts to create more mono-energetic x-rays by using the characteristic Kα emission radiation of certain anode metals, like copper, silver or molybdenium. But generally tungsten is much more widely used especially for in-vivo scanning which demands shorter acquisition and higher x-ray energies or the measurement of bone structures.

This has significant influence in imaging soft tissues. Profiles of tissues with rather similar attenuations cannot be resolved sufficiently, resulting in similar gray values after reconstruction. One way to optimize these profiles, and to improve the image resolution of tissues with similar gray scales, is to use metal filters to block specific ranges of the x-ray spectrum. The filter quality is dependent on the material used and on its thickness. For example, 0.5mm aluminum significantly filters the emission spectrum from <10kV to about 25kV. In contrast titanium (25 micron thickness) shows a significant peak at 7kV. (Figure 5). Other materials used are copper, tin and other metals in various thicknesses depending on the energy to be eliminated. In any soft tissue imaging, including the lung, the right choice of filter and of scanning parameters (kV and µA) are necessary.

D. Detector characteristics

The physical parameters of the detectors/cameras are also of critical importance. These determine the resolution of the scanner. The field of view (FOV) that can be covered, namely the x-y field of view and the z-axis coverage, is also determined by the detectors. Modern high resolution CCD cameras are comprised of an element size of a few µm. The CCD matrix range up to 4kx4k in the newest generation of commercial micro-ct scanners. A typical system comprises a 10 Megapixel CCD (4000x2300effective pixels), with a 12bit dynamic output and a 6.7micron pixel size at the CCD surface. The CCD is coated with a thin layer of a material that is capable to converting x-ray photons into visible light. In many cases gadolinium oxide is used; this has a very specific sensitivity curve (Figure 6). Other materials used for x-ray to light conversion include cesium iodine.

A further critical parameter is the read-out time of the signals. The shorter the read-out time the better the temporal resolution per single exposure. A typical CCD system has a read-out time of a minimum of 100-200 ms. This is of importance for in-vivo scanning of moving targets such as the lung. A mouse breathes with a rate up to 180 times per minute. Even with sedation the respiratory rate is around 60 per minute. Even if a detector with a very fast read-out time is available (in the range of ms), a measurable amount of photons is required to create reasonable images. Therefore this is again a significant trade off: to improve image quality the x-ray dose has to be increased. Often the x-ray tube is not capable of delivering the necessary amount of photons or the applied dose has significant impact on the animal health when long term repeated in-vivo scanning is needed (see next section). One way of scanning the breathing lung is to gate

the micro-CT to the respiratory cycle. A respiratory gated scan takes significantly longer than a non-gated scan when the same scan parameters are used.

There is a new generation of in-vivo scanners now commercially released, that comprise of a read-out time of 20ms but with a accordingly limited spatial resolution (100µm and above). These scanners are typically used in combination with functional imaging methods like µPET and other nuclear methods or to study dynamic processes.

From the physical basics discussed above we may conclude that the total x-ray sensitivity of a micro-CT system is a function of electron energy (x-ray production), the filtering (to enhance or delete certain spectra) and finally the x-ray absorption sensitivity of the x-ray converter at the CCD detector.

E. Comments on dose exposure

As described in a paper on quality limits of micro-CT (32), the linear attenuation coefficient is proportional to (dose)-1/2 and to the (isotropic voxel size)-2 in the reconstructed volume. Therefore an improvement in the precision can be achieved only by increasing the isotropic voxel size (thereby decreasing the resolution of the image) or by increasing the x-ray dose. A lower spectral energy will provide a higher contrast image with a micro-CT system, but there will be fewer photons reaching the detector to form the image.

This dose is approximately 1% of LD50/30 for a mouse (9 Gy). The LD50/30 is a measure of lethal dose to 50% of the population after 30 days. The influence of dose exposure in an experimental situation is not well explored, and there are questions regarding the possible changes that x-ray exposure could have on long term in-vivo studies. Certainly, however, the frequency and duration of micro-CT studies will have significant influence on the mouse biology in the living animal.

F. Resolution of the systems

In medical computed tomography as well as with micro-CT we distinguish between spatial and contrast resolution, i.e. the ability to distinguish between different densities. Spatial resolution is generally quantified in terms of smallest separation at which two points can be distinguished as separate entities. The limiting value of the resolution is determined by the design and construction of the system and by the amount of data and sampling method. There are methods available to measure the spatial resolution directly, as well as indirect methods to calculate the resolution of a system. The indirect methods are somewhat more objective compared to the direct ones.

The geometrical resolution can be represented by the modulation transfer function (MTF). Basically the MTF is the ratio between the true dimension of the object and the resolution of the images acquired. It is calculated usually from the measurements of a

thin wire phantom which provide the point spread function of the system. A given point spread function is used to calculate the MTF. The MTF curves describe the ratio of the contrast in the CT or micro-CT image to the contrast in the object with respect to the spatial frequency. The MTF demonstrates the frequency components of a structure in line pairs per millimeter (lp/mm). Normally the MTF and therefore the resolution of a CT system is evaluated at 10% contrast difference (Figure 7).

G. Tomographic reconstruction

Micro-CT typically utilizes cone beam geometry and is thus true "volume CT". The term "volume CT" or "volumetric CT" has been used in association with the Mayo effort to build the Dynamic Spatial Reconstructor (DSR) (33). Recent emergence of multislice row (MDCT) scanners are moving towards the use of true cone beam geometry. Micro-CT offers a unique testing ground for the future of the mathematics and the image processing needs of clinical scanners.

Early spiral CT scanners (34) provided stacks of cross sectional CT sections. However, the slices were separated in time. The DSR acquired all of the slices simultaneously but cone beam reconstructions were prohibitive of computation time. Tomography slices in medical CT have until recently been generated from 1-dimensional projections via fan-beam methods.

A "true" volume scanner uses 2-dimensional radiographic projections that are collected via CCD cameras or other high-resolution detector arrays. The projection images are collected from different angles of view to generate the necessary volume dataset for the subsequent slice reconstruction. There are two different methods developed: Either the object rotates and the x-ray source and the detectors remain fixed or the x-ray-detector unit rotates and the scanned object remains fixed. Thus in micro-ct the fan-beam geometry is opened to a "pyramid like" or cone beam geometry (Figure 8). This new geometry needs a much more elaborative reconstruction algorithm to calculate slices from the shadow image volume data set: the so-called cone beam algorithm (Feldkamp algorithm, (35)). As the volume data set is acquired via 2-dimensional projections a much higher resolution (Figure 9) can be achieved when compared to fan-beam geometry. Basically the reconstructed slices comprise of the same resolution in all three spatial dimensions. This serves to accommodate oblique reconstructions and other approaches to volumetric exploration of the data.

Even today the reconstruction itself is a problem in micro-CT scanning as it is very computationally expensive. On a conventional PC (3GHz processor, 1GB RAM) a reconstruction of a 1000x1000x1000 cube can take several hours. Various companies are now specialized in providing workstation clusters with highly effective programs and algorithms to reconstruct high-resolution volumes in a reasonable time, thus reducing the reconstruction time to a few minutes for a 1000x1000x1000 cube. To maximize the utility of micro-CT to evaluate animals over time, under multiple physiologic conditions and to explore many animal in a short period of time it is critical that reconstruction times

be, at worst, in the order of hours not days. There must also be the facility to reconstruct image data at low resolution in near real time if one is to be able to adjust experimental protocols based upon observations made at the time of the study.

H. Ring artifact reduction

Ring artifacts can appear due to defective detectors or non-linearities of the detector system. Another reason can be the drift of the detectors sensitivity between white field calibrations or small misalignments in the scanner's center of rotation. These artifacts are undesirable because they may interfere with the qualitative and quantitative analysis of images.

Additional processing of the shadow images before the tomographic image reconstruction process can help to reduce the ring artefacts (36). Examples of such artefacts are shown in Figure 10.

I. Beam Hardening

As a consequence of the polychromatic x-ray source, used in micro-CT and in medical CT, the attenuation is no longer a linear function of absorber thickness. If this nonlinear beam hardening effect is not compensated, the reconstructed images will be corrupted by cupping artifacts. The effect causes different gray value attenuation on normally homogeneous objects (such as phantoms) or wrong determination of gray values (Figure 11). Especially in lung imaging the exact determination of gray values is of crucial interest as it is the only method to gain access to structural changes caused by diseases when structure per se is not visible. In the case of in-vivo scanning, because of scan time and physiologic motion, it is not likely that one will see alveolar level structure as discussed later in this chapter. Reconstruction allows the limitation or deletion of the beam hardening effect. This turns out to be a crucial step: a too low or too high chosen parameter can lead to misleading gray value distribution that can lead to a wrong quantification of tissue types. Medical CT scanners offer sophisticated methods for automated Hounsfield Unit (x-ray attenuation estimates) calibration depending on the protocols used.

It is essential to take care of this effect when analyzing grey values quantitatively because the beam hardening correction influences the gray value calibration significantly. A current project deals with the automatization of Hounsfield Unit (HU) calibration taking into account various scan protocols and their relating beam hardening corrections.

J. Hounsfield Unit calibration

Although a micro-CT is capable of having a resolution of a few µm or less, this may not be sufficient to image the structures of interest. In Figure 12 we demonstrate the effect of

imaging with a voxel size of 35mm, 18mm and 9mm. Further with in-vivo scanning both image acquisition time and spatial resolution are critical. Under these circumstances, the images may not be highly detailed, but still can provide an average grey value representation of the underlying structure. This data may be very informative with regards to the presence or absence of disease. Reasonable HU calibration is thus a prerequisite for meaningful data analysis. The noise inherent to the system of the data makes the HU calibration to a great challenge. Typical grey value distributions are in the range of +- 50 HU and worse depending on the system and protocol used. Currently HU calibration can be a time-consuming project that cannot be performed automatically for several manufacturers. The lack of attention to HU calibration is in part historic. Micro-CT scanners were initially built for the micro-chip industry and the demands in orthopaedic research where detection of high contrast structures was the primary goal.

K. Commercially available systems

Currently, there are six major manufactures of micro-CT scanners, which are alphabetically Bio-Imaging Research (http://www.bio-imaging.com), Enhanced Vision Systems (http://www.gemedical.com/Preclinical_Imaging) recently acquired by GE Medical Systems, ImTek (http://www.imtekinc.com) recently aligned with Philips Medical, ScancoMedical (http://www.scanco.ch/), SkyScan (http://www.skyscan.be), and Stratec (http://www.stratec-med.com/). See Table 1. There are numerous investigators who have built their own custom designed systems.

III. Small animal lung imaging

Micro-CT is becoming a very important tool for small animal imaging, especially for the mouse. Different techniques have been proposed to image small anatomical structures using micro-CT and synchrotron x-ray CT. Synchrotron radiation x-ray sources offer high photon intensity, good collimation and a broad continuous energy range from which any desired spectral region can be selected. A scanner based on a synchrotron source, which provides monochromatic and parallel x-ray beams, gives performance close to the theoretical limits and thereby opens new directions for medical imaging. This method utilizes mono-energetic x-rays at considerable high doses and therefore the spatial resolution is superior to conventional micro-CT. There are currently a few studies describing synchrotron CT used for analysis of lung structures (37), (38), (39), (40). All micro-CT techniques allow a non-invasive evaluation of various anatomical structures such as the trabecular structure of bone which is important for osteoporosis research. The analysis and quantification of bone growth and bone repair models, and the analysis of cardiac vascularization in mice and rats are other current research topics.

Only a few papers have dealt specifically with micro-CT imaging of the lung. Areas of interest include the evaluation of chemically fixed lungs, such as sheep or pig lungs to analyze the 3D morphology of alveolar structures (41). Another group has developed a special lung airway contrasting method in excised rat lungs (42), (43). Three-

dimensional reconstructions showed branching and merging bronchi ranging from 500 to 150 μm (the airway generation=8–16). The morphometry of the small airways (diameter, length, branching angle and gravity angle between the gravity direction and airway vector) was analyzed using a three-dimensional thinning algorithm. The diameter and length exponentially decreased with the airway generation. These results are comparable to those found by our group. Another research group is focusing more on the micro-CT analysis of lung nodules, in particular the micro-architecture of lung nodules to distinguish between benign and malignant nodules (44). As preliminary results they show correlation between light microscopy and micro CT images and suggest the potential as a clinical examination tool. Another paper is published that deals with pulmonary arterial distensibility in excised rat lungs imaged with micro-CT (45), (46). The researchers used perfluorooctyl bromide to enhance x-ray absorbance. The vessel diameters were obtained by fitting a functional form to the image of the vessel circular cross section. The diameter measurements obtained over a range of vascular pressures were used to characterize the distensibility of the rat pulmonary arteries.

A different and new challenge is soft tissue imaging, especially in-vivo lung imaging with micro-CT (47). If motion artifact reduction technologies can be incorporated to solve the problems caused by the long scan time required for an in-vivo micro-CT, soft tissue such as the lung and micro vessel imaging seems to be possible. Our goal is to establish micro-CT, its image reconstruction, protocol optimization and image analysis and postprocessing as a validated tool in small animal lung imaging. A major interest of our group is imaging the small airways using in-vivo scanning techniques as well as evaluating changes in chronic asthma and in various emphysema mouse models. We expect to develop a mouse lung atlas to compliment our growing human lung atlas, based on micro-ct imaging information. As shown in figures 13 and 14, with volume visualization techniques it is possible to create impressive volumetric images of the lung. However, of great importance is to assure the quantitative accuracy of the images and to develop techniques that make use of this quantitative accuracy.

A. Optimized in-situ and in-vivo mouse lung protocol

1. In-situ scanning protocols

We have developed the methodology for scanning the murine lung in-situ and in-vivo, including optimizing micro-CT acquisition and reconstruction parameters, using in situ scans on recently killed mice. Scanning has been performed using the Skyscan 1076 in-vivo micro-CT scanner. Mice, following sacrifice, were intubated tracheally and the lungs inflated with a positive lung air pressure (20cm H2O). For scanning, each mouse was placed in a customized bed constructed of expanded polystyrene foam of medium density (Styrotech, Wolverhampton, UK) so as to minimize extraneous and asymmetric x-ray absorption and beam hardening associated with the sample holder.

One objective of the thoracic scans of the mice is the assessment of emphysema on the basis of measured Hounsfield unit (HU) density within specified volumes in the lung.

Protocols for scanning and reconstruction have been developed for the accurate measurement of HU density irrespective of location inside or outside the mouse thorax, unbiased by beam hardening artifacts. This has been validated by checking for equal HU measurements of air in tracheal cavities and outside the thorax, on the reconstructed cross section images.

Beam hardening has been minimized by several means. An x-ray voltage of 50kV and filtration by 0.5 mm aluminum, in combination with the x-ray absorption efficiency profile of the gadolinium oxide scintillator at energies below 50kV (exponential-like increase with decreasing energy), combine to produce an effective energy spectrum (as measured by the camera) which is reasonably thin and approximately normal. Software correction of beam hardening (the application of a power-law density response curve) in the reconstruction process has been calibrated by scanning a tube of water approximating the width of the mouse thorax (2 cm). Employing these scanning and reconstruction parameters, two protocols have been established, one at 35 micron and one at 18 µm nominal resolution (pixel size), with acquisition times of 20 and 40 minutes respectively. The scanning acquisition is over 360 degrees, and the rotation steps for the 35 µm pixel and 18 µm pixel scans are 0.45° and 0.6° respectively. Note that contrast resolution of low density structures is enhanced by using the lower kV range.

Considerably more work is necessary to identify optimal trade-offs between improved image quality and scanning times. There is a need to establish image analysis methods. An iterative approach to scan protocol development will need to take into consideration, the methods that can accommodate image reconstruction noise and increased or decreased spatial resolution.

Micro-CT appears a useful tool to scan ex-vivo, fixed mouse lungs with sufficient spatial resolution in terms of spatial resolution grey value dynamics and noise because there are no temporal constraints. There are no motion artifacts due to lung decay or fluid shifts which occur with in-situ lung scans, therefore the exposure time can be significantly increased. Thus it is possible to facilitate the 9µm pixel resolution protocol of the Skyscan 1076 scanner. Optimized protocols for the fixed mouse lung with different spatial resolutions are being developed further. The basic characteristics of the 9µm protocol are: scanning time about 120 minutes, no filter, 50kV and 200 µA. Scan protocols are under development to follow in-vivo mice lung changes over a time course. Varying degrees of spatial and density resolution are utilized depending upon the course of disease progression, and guided by pulmonary function measures obtained through such measures as the Scireq ventilator/pulmonary function system. It is of particular note that in-situ lungs of freshly killed mice do not remain stationary when one is working in the micron scale. Tissues continue to relax and decay and fluid volumes continuously shift. To minimize this problem the lung is maintaining inflated by application of continuous positive pressure at the trachea during scanning. Images of lungs in frozen mice have been unsatisfactory to date. We suspect that this is due to crystallization of water in the alveoli.

2. In-vivo scanning protocols

In-vivo scanning is much more complicated and involved than ex-vivo or in-situ scanning. The necessary setup includes full anesthesia equipment, physiologic monitoring and scanner gating possibilities. The physiologic monitoring and control system may consist of some or all of the following components:

- Camera for real time animal's visualization during scanning,
- Real-time local body movement detection for non-contact scanning synchronization with breathing,
- Air / gas flow sensor for scanning synchronization with breathing,
- Sensor for animal temperature measurement,
- Animal's heating by airflow on the object bed,
- ECG-amplifier
- Signals derived from a mechanical ventilator

In-vivo lung scanning is a challenge to the scanner setup: It requires the shortest possible scan times to avoid motion artifacts. There are certain limitations on the dose required to minimize image noise when gray value estimation is required. Current systems require significant trade offs in these matters. The dose exposure may be importance to the animal’s health in long term repeated in-vivo studies.

Optimization of micro-CT protocols in terms of scan time, signal to noise ratio, and spatial resolution are of critical issue. Many parameters have to be taken into account to obtain “best possible” images. Figure 16 shows an 18mm and a 35 mm in-vivo respiratory gated scan. When the breathing of a mouse during anesthesia is sufficiently regular it is also possible to gate the scanner to the spontaneous breathing (Figure 17).
A careful HU calibration has to be performed when the interest of the study lies in determining and quantifying parenchymal changes and relies on estimating partial volume contributions of underlying structures to voxel densities.

B. Examination of lung tissue samples from larger animals

Micro-CT can certainly be used to examine lung tissue samples from larger animals or humans. Structure and grey-scale derived texture can be assessed. In an example presented here, emphysema was induced with papain instillation into sheep lung. In a medical MDCT scanner the lung was examined and with histogram methods emphysematous regions were determined. After lung fixation samples of various regions of the lung suspected of being emphysematous or normal were taken in order to scan them via micro-CT. The resultant micro-CT data are shown in figure 15.

C. Dynamic imaging: Microfluoroscopy coupled to micro-CT

Because of the long scanning time needed to image the multiple angles of view used in micro-CT, it is not possible to image dynamic processes such as blood flow or ventilation as is possible with current MDCT scanners whose rotation times are on the order of 0.33 seconds for a full 360 degree rotation. An alternative approach is to simply utilize a single view from the micro x-ray imaging system to study physiological processes and to then relate these processes to 3D anatomy by imaging the many angles of view needed for CT reconstruction at the completion of the single view study.

The Keck Imaging Laboratory at Marquette University has a particular interest in using in-vivo and ex-vivo lung preparations to describe structure-function relationships involved in control and modulation of the pulmonary circulation in the normal and diseased lung. Since hypoxic vasoconstriction is generally considered to be the major physiological local blood flow controlling system in the lungs, the x-ray imaging system described below has been used to address a variety of questions related to structural and functional consequences of hypoxia. For example, the group has examined how the geometric and mechanical properties of the pulmonary vasculature respond to both acute hypoxia and chronic exposure to hypoxia that has been shown to result in vascular remodeling (48), (49), (50). Of particular interest is how the changes in these properties affect the longitudinal and parallel distributions of stresses and strains on and within the vessel walls (51), (46), (50). The overall strategy has been to combine dynamic planar angiographic imaging at several resolutions with high-resolution micro-CT imaging of the vascular structure.

The system is illustrated in the upper panel of figure 3. The spatial capabilities are illustrated in Figure 18, showing projection images of an isolated rat lung with the arterial free filled with perfluorooctyl bromide (providing x-ray contrast) at three magnification levels. The ability to image and quantify vascular structure of the entire lung as well as particular regions at very high resolution is illustrated. Although this approach is extremely useful for examining vessels as small as 20mm in the periphery of the lung, the overlap of vessels in the projection images renders this approach problematic for reliably measuring all visible vessels. However, rotation of the specimen within the beam enables acquisition of projection images that are used for 3D volumetric CT reconstruction as shown in Figure 19. These images have then been used to characterize the morphometric structure of vessel trees by measuring vessel lengths, branching angles, and diameters. In addition, limited functional information is obtainable. For example, modulating the vascular and airway pressures can characterize distensibility via pressure-diameter relationships (45), (50). Examination of the response of different segments of the vasculature to various pulmonary vasodilators or vasoconstrictors (52), (53) is also possible.

Overall and regional pulmonary vascular function has been assessed using dynamic projection angiography (54). Figure 20 illustrates three time frames extracted from a sequence of images of a region of a dog lung obtained during passage of a bolus of x-ray contrast medium. Regions of interest positioned over artery and vein pairs as well as the

surrounding microvasculature, yield time-absorbance curves that were used to determine the effects of alveolar hypoxia on pulmonary microvascular volume (49). Absorbance data during both normoxic (alveolar gas 15% O2) and hypoxic (5% O2) conditions were collected and analyzed to obtain arterial inlet and venous outlet time-absorbance curves from which total pulmonary vascular volume was calculated. Microvascular regions (vessels smaller than ~40 mm) were measured from high magnification image sequences and the fractional change in microvascular volume from normoxia to hypoxia was determined from the area under the microvascular absorbance curves. Hypoxia decreased total lobar volume by about 13% and microvascular volume by about 26%. Given the morphometry of the lung vasculature, this suggests that capillary volume was substantially decreased by hypoxia. The physical explanation is not apparent, but since flow was held constant, simple narrowing of arteries would not be expected to decrease capillary pressure, although an active change in capillary dimensions may be possible.

Angiographic studies were also used to address the question of how the complex routes the blood can take through the lungs actually produce the overall pulmonary vascular transport function (distribution of transit times), which is important for studies of organ function. A common visualization of transit time dispersion in conducting trees has been based on the assumption that flow through any connecting segment is proportional to the number of terminals subtended by that segment, and that the transit time through each segment is its volume divided by its flow. One consequence of these assumptions is that short pathways would have short transit times and long pathways would have long transit times, so that the transit time distribution would be close to a scaled distribution of path lengths. The contribution of the pulmonary arterial and venous trees to the whole lung transport function was examined by measuring time-absorbance curves from selected pulmonary arteries and veins and revealed that path length contributed remarkably little to the dispersion of lung transit times (55). This result contradicted the common visualization referred to above and showed instead that the bolus arrived at an artery of a given diameter at about the same time regardless of the wide range in distances it had to travel to reach each vessel of that diameter. This observation can be explained by assuming that despite the apparent complexity of the arterial branching pattern, at each asymmetric bifurcation, the faster streamlines tend to pass through the larger diameter daughter branch, while the smaller daughter receives the slower streamlines. In other words, the streamlines with low velocity at the inlet, which are also closest to the vessel wall, pass into small branches serving short pathways, while the higher midstream velocity streamlines continue on through the larger branches to long pathways. Thus, the arterial transit time distribution is not a reflection of the path length distribution, but instead the path length distribution and branching pattern are matched to the vessel velocity profiles so that near uniformity in arterial transit times is achieved.

Progress is being made toward combining static micro-CT data, which provide vessel structure and distensibility, with dynamic projection angiography at high resolution for measuring the contribution of vessel tone, regardless of the interaction of tone and vascular remodeling on hemodynamic function. Future enhancements of micro-CT scanners are moving in the direction of improved spatial resolution but also perhaps more importantly towards increased temporal resolution for improved functional applications.

A tour-de-force example of dynamic micro x-ray-based imaging is demonstrated in figure 21. Here a ground beetle was scanned via a synchrotron x-ray source and the projection data allowed researchers to follow the dynamic properties of the tubular respiratory apparatus. (56)

D. Conclusions

Imaging the in-situ mouse lung is a feasible task although specific scanning parameters have to be taken into account. Significant compromises of spatial resolution and scan time are required. We discuss methods of achieving optimal images over a reasonable scan time, i.e.: within the time before the lung is undergoing postmortem destruction. Quantification issues are still being resolved. In-vivo scanning is an even more challenging procedure which includes anesthesia to be maintained throughout the scan, triggering of the CT, physiologic monitoring, etc. We present recent results in our laboratory indicating that meaningful in-vivo imaging is feasible, allowing for longitudinal studies in the same mice. These recommendations are summarized below in relation to our current experience with a Skyscan 1076 system.

- Imaging with 35 and 18 micron on a side voxel resontruction in-vivo is possible in an anesthetized mouse, with recovery
- If HU's are well calibrated, 35 mm scans with inherent physiologic motion artefacts in-vivo will be useful to estimate underlying structural changes using density and texture information
- 18 micron in-situ (post mortem) imaging provides anatomic detail suitable for airway wall measurements
- 9 micron ex-vivo imaging provides anatomic detail suitable for alveolar level visualization
- In-vivo imaging can provide detail suitable for lung volume measurements and may provide detail suitable for lung density measurements.
- Efforts must be guided towards providing accurate Hounsfield Unit calibration for in-vivo study to be of maximum utility.
- In table 2 we provide our method for lung fixation

Note: all values above represent isotropic voxel dimensions

Micro-CT imaging not only allows for the study of lung anatomy down to the alveolar level, but it provides the testing ground for improved cone beam algorithms which can translate up to future clinical scanners. Micro-CT imaging has seen a rapid transition from one of a kind laboratory instruments to commercially developed systems which have moved from use in the study of high contrast static structures such as post mortem specimens of bone towards more recent interest in imaging structural changes over time in vivo. A small but growing number of applications have now sought to study soft tissue structures and a number of manufacturers have begun to market what they call in-vivo scanners. It has become clear that much work is necessary to develop the scanners and

the image handling to accommodate the special needs of soft tissue imaging and particularly soft tissue imaging in-vivo. If we are to rely on imaged grey scale and grey scale texture to assess changes in the lung periphery in-vivo as a marker of micro structural changes over time with eventual post mortem imaging to verify micro structural changes, we must be able to rely on the accuracy of the soft tissue attenuation coefficients and the scanner's grey scale sensitivity.

The combination of micro x-ray fluoroscopy and micro-CT, offers in new insights into structure to function relationships in the lung. This will be further enhanced with the introduction of multi-modality protocols utilizing various combinations of technology as are outlined in the other chapters of this book.

Data management and image processing of micro CT volumes remain challenging: One volumetric image of the mouse lung in 9um pixel resolution can be as large as 30Gb. The visualization and meaningful data analysis software development would be facilitated by a move to a PC based upon a 64bit processor with maximized RAM. New strategies in image processing and analysis will have be defined by close collaboration with investigators in computer science and biology. Imaging on a regular basis with subsequent analysis and storage will require an addition of large disc farms.
With anticipated progress in hardware and software technology, mouse micro-ct imaging will become a common reality.

E. Literature

1. Hoffman EA, McLennan G. Assessment of pulmonary structure-function relationships and clinical outcomes measures: Quantitative volumetric CT of the lung. Academic Radiology 1997;4(11):758-776.
2. Hoffman EA, Reinhardt JM, Sonka M, Simon BA, Guo J, Saba O, Chon D, Samrah S, Shikata H, Tschirren J, Palagyi K, Beck KC, McLennan G, Characterization of the interstitial lung diseases via density-based and texture-based analysis of computed tomography images of lung structure and function. Academic Radiology 2003;10(10):1104-1118.
3. Hoffman EA, Sinak LJ, Robb RA, Ritman EL. Noninvasive quantitative imaging of shape and volume of lungs. J Appl Physiol 1983;54(5):1414-1421.
4. Shikata H, Hoffman EA, Sonka M. Automated segmentation of pulmonary vascular tree from 3D CT images. Progress in Biomedical Optics and Imaging 2004;5(23):107-116.
5. Tschirren J, Hoffman E, McLennan G, Sonka M. Airway tree segmentation using adaptive regions of interest. Progress in Biomedical Optics and Imaging 2004 2004;5(23):117-124.
6. Bilgen D, Hoffman EA, Reinhardt JM. Segmentation and analysis of human airway tree from 3D X-Ray CT images. IEEE Trans Med Imaging in press.
7. Hu S, Hoffman EA, Reinhardt JM. Automatic lung segmentation for accurate quantitation of volumetric X-ray CT images. IEEE Trans Med Imaging 2001;20(6):490-498.
8. Wood S, Hoford J, Zerhouni E, Hoffman E, Mitzner W. Quantitative 3-D reconstruction of airway and pulmonary vascular trees using HRCT. Biomedical Image Processing and Biomedical Visualization 1993;1905:316-323.
9. Tschirren J, Palágyi K, Hoffman EA, Sonka M. Segmentation, Skeletonization, and Branchpoint Matching - A Fully Automated Quantitative Evaluation of Human Intrathoracic Airway Trees. In: Dohi T, Kikinis R, editors. Proceedings of Fifth International Conference on Medical Image Computing and Computer Assisted Intervention; 2002; Tokyo, Japan: Springer-Verlag Berlin Heidelberg; 2002. p. 12-19.
10. Hoffman EA, Acharya RS, Wollins JA. Computer-aided analysis of regional lung air content using three-dimensional computed tomographic images and multinomial models. Int J Mathem Model 1986;7:1099-1116.
11. Tawhai M, Hunter P, Tschirren J, Reinhardt J, McLennan G, Hoffman E. CT-based geometry analysis and finite element models of the human and ovine bronchial tree. J Appl Physiol 2004;in press.
12. Hoffman EA, Ritman EL. Effect of body orientation on regional lung expansion in dog and sloth. J Appl Physiol 1985;59(2):481-491.

13. Tajik JK, Chon D, Won C, Tran BQ, Hoffman EA. Subsecond multisection CT of regional pulmonary ventilation. Acad Radiol 2002;9(2):130-146.

14. Chon D, Beck K, Shikata H, Larsen R, Hoffman EA. Regional pulmonary blood flow by dynamic multi-slice x-ray CT. J Appl Physiol 2004;in press.

15. Chulho W, Chon D, Tajik J, Tran B, Robinswood G, Beck K, Hoffman EA. CT-based assessment of regional pulmonary microvascular blood flow parameters. J Appl Physiol 2003;94:2483-2493.

16. Tomimitsu S, Samrah S, Hoffman E, Beck K, McLennan G. Lung Preparation Technique for Computed Tomography-Pathologic Correlation. American Journal of Respiratory and Critical Care Medicine 2003;167(7):A875.

17. Samrah S, McLennan G, Chon D, Beck KC, Ross A, Hoffman EA. Multi-Row Detector CT-Based Measures of Microvascular Mean Transit Times and Parenchymal Texture as an Early Marker of Inflammatory Processes Leading to Emphysema. Am J Respir Crit Care Med 2003;167(7):A874.

18. Irvin CG, Bates JH. Measuring the lung function in the mouse: the challenge of size. Respir Res 2003;4(1):4.

19. Shapiro SD. Animal models for chronic obstructive pulmonary disease: age of klotho and marlboro mice. Am J Respir Cell Mol Biol 2000;22(1):4-7.

20. Jorgensen S, Demirkaya O, Ritman EL. Three-dimensional imaging of vasculature and parenchyma in intact rodent organs with X-ray micro-CT. Am J Physiol 1998;275(3, Pt 2):H1103-1114.

21. Ritman EL. Molecular imaging in small animals--roles for micro-CT. J Cell Biochem Suppl 2002;39:116-124.

22. Ritman E. Micro-computed tomography-current status and developments. Ann RevBiomed Eng 2004;6:185-208.

23. Ruegsegger P. Imaging of Bone Structure. In. Second ed. Boca Raton: CRC Press; 2001:1-24.

24. Paulus M, Gleason S, Kennel S, Hunsicker P, Johnson D. High resolution X-ray computed tomography an emerging tool for small animal cancer research. Neoplasia 2000;2 (1-2)(Jan-Apr):62-70.

25. Paulus M, Sari-Sarraf H, Gleason S, Bobrek M, Hicks J, Johnson D, Behel J, Thompson L, Allen W. A new X-ray computed tomography system for laboratory mouse imaging. IEEE Transactions on Nuclear Science 1999;46(3):558-564.

26. Durand, Ruegsegger P. High contrast resolution of computed tomography images for bone structure analysis. Medical Physics 1992;19:569-573.

27. Sasov A, Van Dyck D. Desktop X-ray microscopy and microtomography. J Microsc 1998;191(2):151-158.

28. Marxen M, Thornton M, Chiarot C, Klement G, Koprivnikar J, Sled J, Henkelman R. Micro CT scanner performance and considerations for vascular specimen imaging. Med Phys 2004;31(2):305-313.

29. Chen LM FP, Toth R, Kieffer JC, Krol A, et al. Laser-based intense hard X-ray source for mammography. Proc SPIE 2003;5030:923-928.

30. Bonse U, Busch F. X-ray computed microtomography (microCT) using synchrotron radiation (SR). Prog Biophys Mol Biol 1996;65(1-2):133-169.

31. Grodzins L. Optimum energies for x-ray transmission tomography of small samples : Applications of synchrotron radiation to computerized tomography I. Nuclear Instruments and Methods in Physics Research, 1983;Volume 206 (Issue 3): 541-545.

32. Ford N, Thornton M, Holdsworth D. Fundamental image quality limits for micro-computed tomography in small animals. Med Phys 2003;30(11):2869-2877.

33. Robb RA, Hoffman EA, Sinak LJ, Harris LD, Ritman EL. High-speed three-dimensional x-ray computed tomography: the dynamic spatial reconstructor. ProcIEEE 1983;71:308-319.

34. Kalender W, Seissler W, Klotz E, Vock P. Spiral volumetric CT with single-breath-hold technique, continuous transport, and continuous scanner rotation. Radiology 1990;176(1):181-183.

35. Feldkamp LA, Davis LC, Kress JW. Pratical cone-beam algorithm. J Opt Soc Am 1984;1(A):612-619.

36. Tang X, Ning R, Yu R, Conover D. Cone beam volume CT image artifacts caused by defective cells in x-ray flat panel imagers and the artifact removal using a wavelet-analysis-based algorithm. Med Phys 2001;28(5):812-825.

37. Fujimoto S, Johkoh T, Koyama M, Ueguchi O, Honda H, Nakamura H. Analysis of Three-dimensional Microanatomy of the Human Lung Tissue Specimens Using Ultra High-Resolution CT with a Monochromatic Synchrotron Radiation System. In: RSNA; Nov 30 – Dec 5, 2003; Chicago; A259

38. Bayat S, Le Duc G, Porra L, Berruyer G, Nemoz C, Monfraix S, Fiedler S, Thomlinson W, Suortti P, Standertskjold-Nordenstam CG, Sovijarvi AR. Quantitative functional lung imaging with synchrotron radiation using inhaled xenon as contrast agent. Phys Med Biol 2001;46(12):3287-3299.

39. Porra L, Monfraix S, Berruyer G, Le Duc G, Nemoz C, Thomlinson W, Suortti P, Sovijarvi AR, Bayat S. Effect of tidal volume on distribution of ventilation assessed by synchrotron radiation CT in rabbit. J Appl Physiol 2004;96(5):1899-1908.

40. Ikura H, Shimizu K, Ikezoe J, Nagareda T, Yagi N. In vitro evaluation of normal and abnormal lungs with ultra-high-resolution CT. J Thorac Imaging 2004;19(1):8-15.

41. Litzlbauer H, Moell C, Neuhauser C, Nachtmann S, Greschus W. Three-dimensional Assessment of Alveolar Tissue by Micro-computed Tomography. In: RSNA; Chicago; Nov 30 – Dec 5, 2003: A259

42. Sera T, Fujioka H, Yokota H, Makinouchi A, Himeno R, Schroter R, Tanishita K. Three-dimensional visualization and morphometry of small airways from microfocal X-ray computed tomography. J Biomech 2003;36(11):1587-1594.

43. Sera T, Fujioka H, Yokota H, Makinouchi A, Himeno R, Schroter R, Tanishita K. Localized compliance of small airways in excised rat lungs using microfocal X-ray computed tomography. J Appl Physiol 2004;96(5):1665-1673.

44. Niki N, Noboru, Kawata Y. Image analysis of pulmonary nodules using micro CT. In: Sonka M, Hanson K, editors. Proc SPIE; 2001; 718-725.

45. Karau KL, Johnson RH, Molthen RC, Dhyani AH, Haworth ST, Hanger CC, Roerig DL, Dawson CA. Microfocal X-ray CT imaging and pulmonary arterial distensibility in excised rat lungs. Am J Physiol Heart Circ Physiol 2001;281(3):H1447-1457.

46. Karau KL, Molthen RC, Dhyani A, Haworth ST, Hanger CC, Roerig DL, Johnson RH, Dawson CA. Pulmonary arterial morphometry from microfocal X-ray computed tomography. Am J Physiol Heart Circ Physiol 2001;281(6):H2747-56.

47. Cavanaugh D, Johnson E, Price R, Kurie J, Travis E, Cody D. In vivo respiratory-gated micro-CT imaging in small-animal oncology models. Mol Imaging 2004;3(1):55-62.

48. Dawson CA, Krenz GS, Karau KL, Hanger ST, Hanger C, LInehan JH. Structure-function relationships in the pulmonary arterial tree. J Appl Physiol 1998;86:569-583.

49. Clough AV, Haworth ST, Ma W, Dawson CA. Effects of hypoxia on pulmonary microvascular volume. Am J Physiol Heart Circ Physiol 2000;279(3):H1274-1282.

50. Molthen RC, Wietholt C, Haworth ST, Dawson CA. Estimation of pulmonary arterial volume changes in the normal and hypertensive fawn-hooded rat from 3D micro-CT data. In: Chen C-T, Clough A, eds. Physiology and Function from Multidimensional Images; 2002:266-275.

51. Johnson RH. Analysis of 3D Pulmonary microangiograms. In: Doi K, MacMahon H, Giger M, Hoffman K, eds. Computer-aided Diagnosis in Medical Imaging. Amsterdam: Elsevier; 1999:369-376.

52. Guarin M, Dawson CA, Nelin LD. The arterial site of action of nitric oxide in the neonatal pig lung determined by microfocal angiography. Lung 2001;179(1):43-55.

53. Bentley J, Rickaby D, Haworth ST, Hanger CC, Dawson CA. Pulmonary arterial dilation by inhaled NO: arterial diameter, NO concentration relationship. J Appl Physiol 2001;91(5):1948-1954.

54. Clough AV, Linehan JH, Dawson C. Regional perfusion parameters from pulmonary microfocal angiograms. American Journal of Physiology 1997;272(3 Pt 2):H1537-H1548.

55. Clough AV, Haworth ST, Hanger CC, Wang J, Roerig DL, Linehan JH, Dawson CA. Transit time dispersion in the pulmonary arterial tree. J Appl Physiol 1998;85(2):565-574.

56. Westneat MW, Betz O, Blob RW, Fezzaa K, Cooper WJ, Lee WK. Tracheal respiration in insects visualized with synchrotron x-ray imaging. Science 2003;299(5606):558-560.

Legends

Figure 1
Shown is a composite representing several methods for quantifying the lung including airway segmentation, airway segment labeling, color coding of blood flow parameters from time series analysis of passage of a bolus of iodinated contrast agent In the upper right inset, we display a mathematical model of the airway tree. This model actually extends out to the terminal bronchi and is generated from a starting segmentation of the lungs and airway tree using CT scanning and this provides a subject specific, complete airway tree model. (Work in collaboration with Merryn Tawhai and Peter Hunter, Auckland, New Zealand) In the lower portion of the image we demonstrate a large animal model (sheep) of lung inflammation leading to emphysema. Images to the far lower right demonstrate color coded images of perfusion showing that at day 16 (lower row) flow pattern abnormalities emerge in the left (shown on the right of the image), untreated lung while grey scale images show no signs of disease. While significant advances have been made in quantitative application for large animal/human CT imaging, micro CT imaging of the lung remains in its infancy. As this chapter outlines, there is much to be done to bring micro CT to the rigorous standards applied in clinical CT both from the standpoint of the hardware, reconstruction software, and image handling.

Figure 2
A conventional medical CT scanner provides a spatial resolution at best of roughly 100mm x 100mm x 750mm voxels. In this example a mouse lung was scanned with a state-of-the-art Siemens system. In contrary to micro-CT the scanning time is much faster: The whole data volume was acquired in about 2 seconds. It is obvious that these methods cannot be used for studying small structures in the lung down to alveolar level.

Figure 3
Basically there are two different methods to construct a micro-CT: Either the x-ray source-detector system remains fixed and the object rotates (a) or the source-detector system rotates around the fixed object (b). The latter is normally used for in-vivo scanners. Figure (a) represents the X-ray imaging system with detector (left), source (right) and stage (center) supporting a mouse or rat. This technique is suitable for very high spatial resolutions down to 1µm. In a special case (described in the text), CT imaging is performed by rotating the specimen within the beam using a typical total scan time of ~2 minutes. Dynamic angiographic projection imaging is performed at 60 frames/second during the passage of a bolus of x-ray contrast medium. Figure (b) shows a commercially available in-vivo scanning system with physiologic monitoring and gating possibilities (Skyscan 1076).

Figure 4
X-ray emission spectrum of tungsten at a maximum electron energy of 100kV with its characteristic peaks at 59,3 kV and 67,2 kV.

Figure 5
X-ray transmission curve of a 0.5 mm aluminum filter: At the lower end of the energy spectrum the transmission decreases and gets x-ray transparent above 30kV. The right image shows the different transmission capabilities of 25 mm titanium filter with its significant peak at 7kV. The data are from: http://www.cxro.lbl.gov/

Figure 6
X-ray energy absorption curve of gadolinium oxide which converts x-ray photons into visible light. CCD cameras or other light sensitive devices measure then the emitted photons. It has a significant input on detector sensitivity as a function of photon energy (data from http://physics.nist.gov/PhysRefData/XrayMassCoef/ElemTab)

Figure 7
Modulation Transfer Function (MTF) of a typical micro-CT system: Note the 10% threshold i.e. the frequency when the contrast has dropped to 10% of the maximum value obtained by 0 line pairs per mm. This system is principally capable to resolve 5 line pairs per mm.

Figure 8
a) The principle geometry of a “fan beam” system: Only one slice is acquired at a time. This acquisition technique is used in clinical CT scanners. In modern multi-detector CT scanners a modified fan-beam algorithm is used.
b) Principle geometry of a “cone beam” system: This method uses full 2-D x-ray profiles (shadow images) to generate a volume data set, a method typical for micro-CT.

Figure 9a,b:
Radiographic projections or shadow images of a mouse acquired with a cone-beam micro-CT at two different angles

Figure 10
Example for ring artifacts in this image of a water phantom (a): During the reconstruction process most of these artifacts can be reduced.
b) Mouse lung scan reconstructed without ring artifact reduction
c) Mouse lung scan reconstructed with ring artifact reduction which results in a significant optimization of the image quality.

Figure 11
Beam hardening correction: A plastic syringe filled with water was scanned with a conventional micro-ct protocol as it is used for in-vivo studies. Figure (a) was calculated without beam hardening correction. Note the changing of the gray values from light near the surface of the syringe to darker in the middle. This effect is not caused by varying attenuation factors of the phantom itself but by the beam hardening effect. It is possible to correct this artifact during the reconstruction process – see image b. In this case the gray values distribute more evenly across the reconstructed image.

Figure 12
A fixed mouse lung was scanned with different scan protocols and reconstructions were calculated at the same position. Different scan resolutions, related reconstruction times and the required memory per slice (for half field of view reconstruction) are shown:
a) 35 mm/voxel, 500 x 500 x 16bit matrix, 0.5 MB per slice, 30 min volume acquisition time, 1 min back projection time per slice
b) 18 mm/voxel, 1000 x 1000 x 16bit matrix, 2 MB per slice, 90 min volume acquisition Time, 2 min Back Projection time per slice
c) 9 mm/voxel, 2000 x 2000 x 16bit matrix, 8 MB per slice, 270 min volume acquisition Time, 7 min Back Projection time per slice

Figure 13
Volume rendering of a fixed mouse lung including the segmented bronchial tree in different angles of view. The airways were segmented using in-house developed software (5) (35µm pixel resolution scan, Skyscan 1076 scanner, AnalyzeAVW software for visualization)

Figure 14
Volume rendering of fixed mouse lungs (25µm effective resolution scan, Imtek micro-CT). The renderings were generated with the amira software package

Figure 15
A sheep was scanned in a conventional CT scanner in order to measure regional blood flow with a dynamic CT protocol. **a)** CT of a sheep lung with subsequent histogram analysis: The lung area marked in green was suspected to be emphysemateous as its overall density was slightly lower than the rest of the lung. **b)** After lung fixation samples were taken on the same level as the CT slices. **c)** Micro-CT of a non-emphysemateous region, 25 mm pixel resolution, 40 minutes scan, 45 kV, 400 µA: the lung tissue structure is rather homogenius. **d)** Micro-CT of the emphysemateous region, 25 mm pixel resolution, 40 minutes scan, 45 kV, 400 µA: The sample shows also a lower density caused by the brake down of alveolar structures. A subsequent histological examination proved that the regions less dense in the micro-ct was slightly emphysemateous because the alveolar structures started already disintegrate.

Figure 16
Comparison of resolution achieved in-situ (dead mouse with lung inflated at constant PEEP level) versus in-vivo (gated to end expiration) scan. Isotropic reconstructed voxel size was 18 microns. The worse signal to noise ratio in the in-vivo scan is mostly caused by the reduced exposure time, i.e. 1770 ms for the in situ scan and 295ms for the in-vivo scan. The reduced exposure time is necessary to minimize motion artifacts.

Figure 17
The figure shows a 35mm in-vivo scan that was gated with spontaneous breathing of the mouse. Here the exposure time per single frame was 158ms.

Figure 18:
Top: Projection images of a rat lung at three magnification levels. The white dashed box on the left image encloses the middle image, and the solid white box on the middle image encloses the right image. The small white rectangles designated by the arrows are the boxes across which the line scans were taken for vessel diameter estimation in the respective lower panels. The solid lines in the lower panels indicate a model fit to the line scan data obtained from the vessel cross section.

Figure 19:
Left: A projection image of a rat lung with arteries enhanced by filling with perfluorooctyl bromide. Middle: A transaxial slice through the reconstructed 3D volume. Right: A surface shaded rendering of the three dimensional volume of the same rat left lung at about the same viewing angle and with the threshold set to eliminate the smallest vessels so the basic tree structure can be seen.

Figure 20:
Top: Angiographic images acquired during the passage of a bolus of contrast medium through a field of view through a dog lung perfused at constant flow. The indicated times are when the change in opacification was maximum in the regions indicated by the artery, a, vein, v, and microvascular, m, boxes. On the left the bolus fills the arteries but has barely begun to reach the capillaries. The background in the middle panel is dark because the bolus has virtually left the arteries and is spread throughout the capillary bed. By 4.9 seconds, the bolus has reached the veins, but it has not yet completely left the capillaries. Bottom: Absorbance curves a and v represent the concentration of contrast material passing through the respective detection sites during normoxic (PO2 = 116 Torr) conditions while m represents the residue curve obtained from the indicated microvascular region during normoxia and hypoxia (PO2 = 39 Torr). Thus m represents the amount of contrast material residing in the microvessels at a given time so that the area under m is proportional to the microvascular volume, which is substantially decreased by hypoxia.

Figure 21:
a) Ground beetle, Platynus decentis, family Carabidae. X-ray images from the beamline at the
Advanced Photon Source, Argonne National Laboratory. Beetle specimen scanned at four points during tracheal compression (two times about 0.5 sec apart). These images demonstrate that beetles rapidly compress and expand the tracheal system in a manner superficially similar to the inflation of lungs.
b) Upper left: Beetle tracheal tubes fully expanded.
c) Lower left: beetle tracheal tubes fully compressed. Beetles and other insects can inhale and exhale 1/2 the volume of the large trachea, similar to the volume of human lungs during mild exercise.
Reproduced by kind permission of M.W. Westneat (56)

Table legends:

Table 1: Some performance characteristics of commercially available micro-CT scanners

Table 2: Mouse lung fixation protocol

Table 1

	Scanco	Skyscan	Imtek	EVS/GE	Stratec	BIR
Scanner Product	VivaCT 40	Skyscan 1076	MicroCAT 2	Explore RS	XCT Research M	Actis Volume CT
X-ray Source	Focal Spot: 5-7μm, 30-70 kV, 160μA	Focal Spot: 5μm, 20kV - 100kV, 40-200 μA	Focal Spot: 9μm, 20kV -130kV, 400 μA	Focal Spot: 2-90kV, 180μA	Focal Spot: 50μm, 45-60kV, 0,2-500 μA	Focal Spot: 3μm, 10-225kV, 0.01-300μA
Detector size	2048x255	4000x2300	4096x4096	2048x2048	12 detectors	1408x1888
Field of View	20-40mm	35mm or 38mm	35mm - 110mm	40mm	50mm	300mm
Spatial Resolution	10μm	9-35μm	15μm	27-90 μm	70-500 μm	12,5 μm
Scan Speed	360s	5 fps	5 fps	180s-900s	80 s	1 - 30 fps

Table 2: Protocol for lung fixation:

I. Mouse preparation

a) Inject mouse with ~0.4 cc anesthetic (Ketamine/Xylazine mixture with 17.5 mg/cc ketamine and 2.5 mg/cc xylazine) and test reflexes on pain

b) Inject barbituate (pentobarbital) to euthanize ~0.15 cc and pin mouse limbs back to begin dissection

II. Accessing Internal Organs

a) Snip skin inferior to xyphoid process (thoracic cavity) and cut in strait line to lateral sides

b) Pull liver downward with small forceps and cut vessels and connective tissue, locate diaphragm and make small puncture on each side

c) Cut diaphragm along ribcage

- Start at puncture mark and cut towards sternum on both sides
- Do not complete cut-leave tissue posterior to sternum

d) Cut sternum and pin back ribs to expose lungs and heart

e) Administer right ventricular injection to perfuse the tissue with 20 cc phosphate buffered saline

III. Tracheal Dissection

a) Dissect tissue with curved hemostats. After dissection of tissue surrounding trachea, a loose knot must be in position to secure placement of 20/22 gage angiocath.

b) Cut knick into trachea superior to 2.0 silk string, insert angiocath. and tighten knot.

IV Lung Removal

Pull tightly and gently on both strings and cut connective tissue surrounding lungs

V. Lung fixation

a) Use Modified Heitzman's Solution: 25% Polyethylene glycol (PEG), 10% ethanol (95%); 10% formaldehyde (37%); and 55% distilled water.

b) Inject trachea with 1cc modified Heitzman's Solution. Then, immerse lungs in modified Heitzman's Solution with a 20 cm above ground tracheal drip for 24 hours.

c) Air dry with 20 cmH2O continuous airway pressure for 24 hours.

d) After lungs are fixed and dried, place them in sealed container at room temperature.

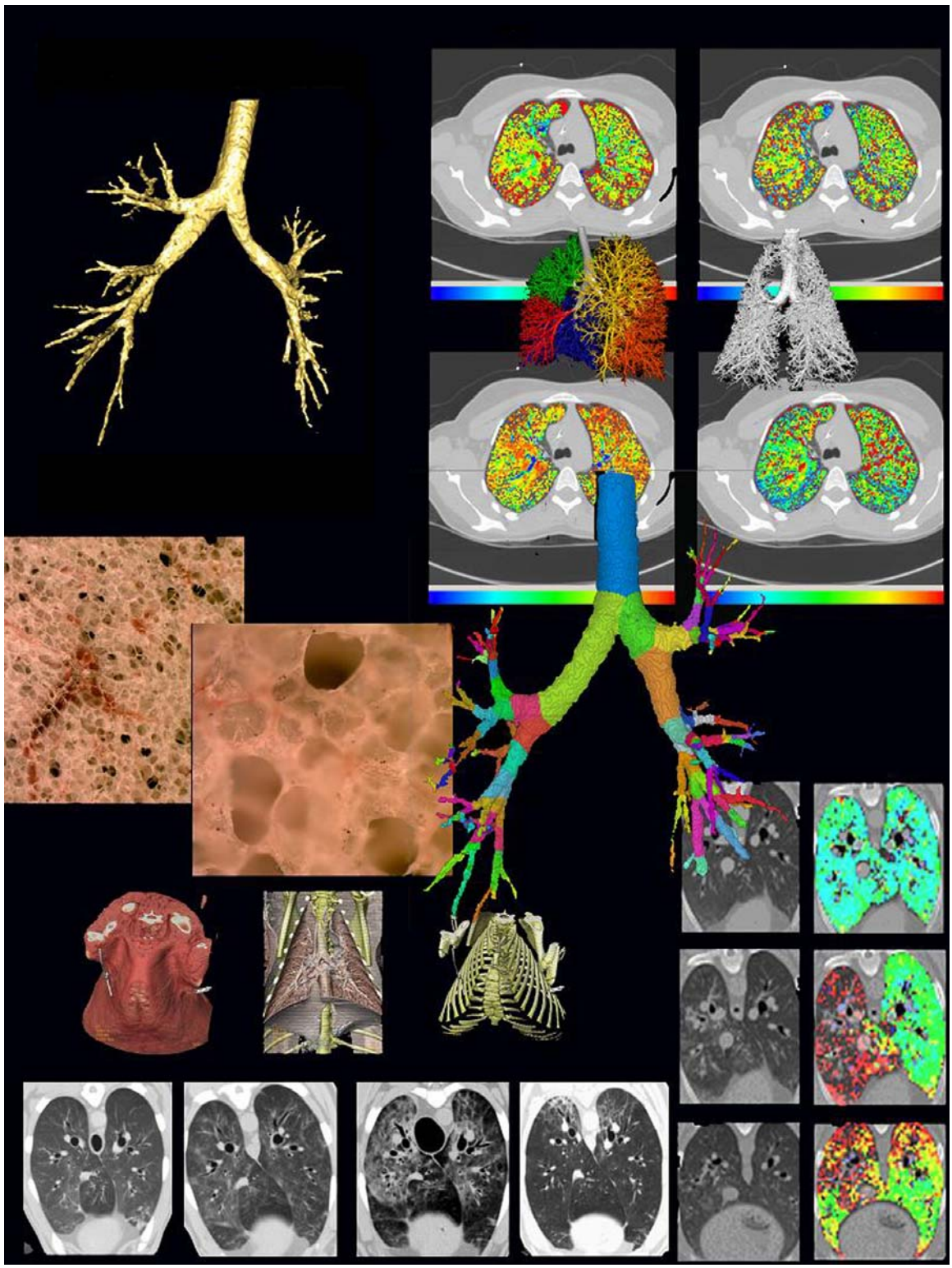

Figure 1

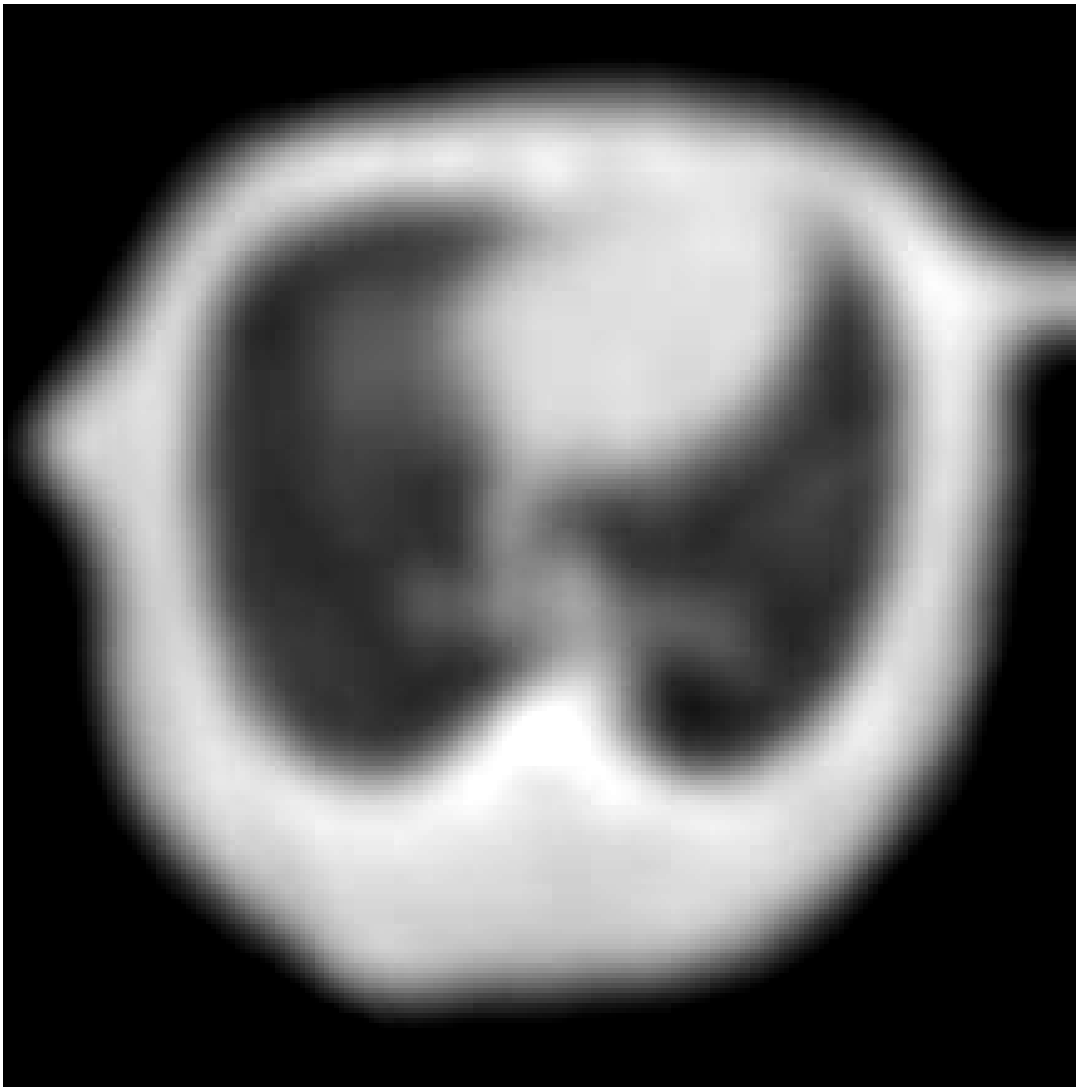

Figure 2

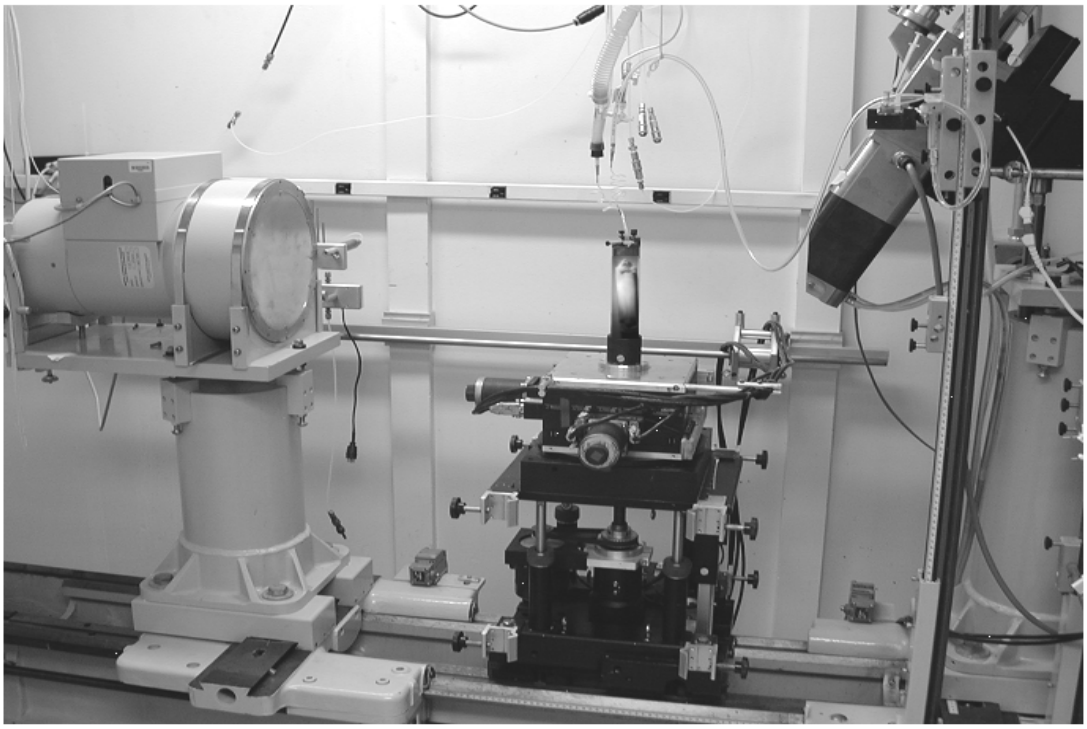

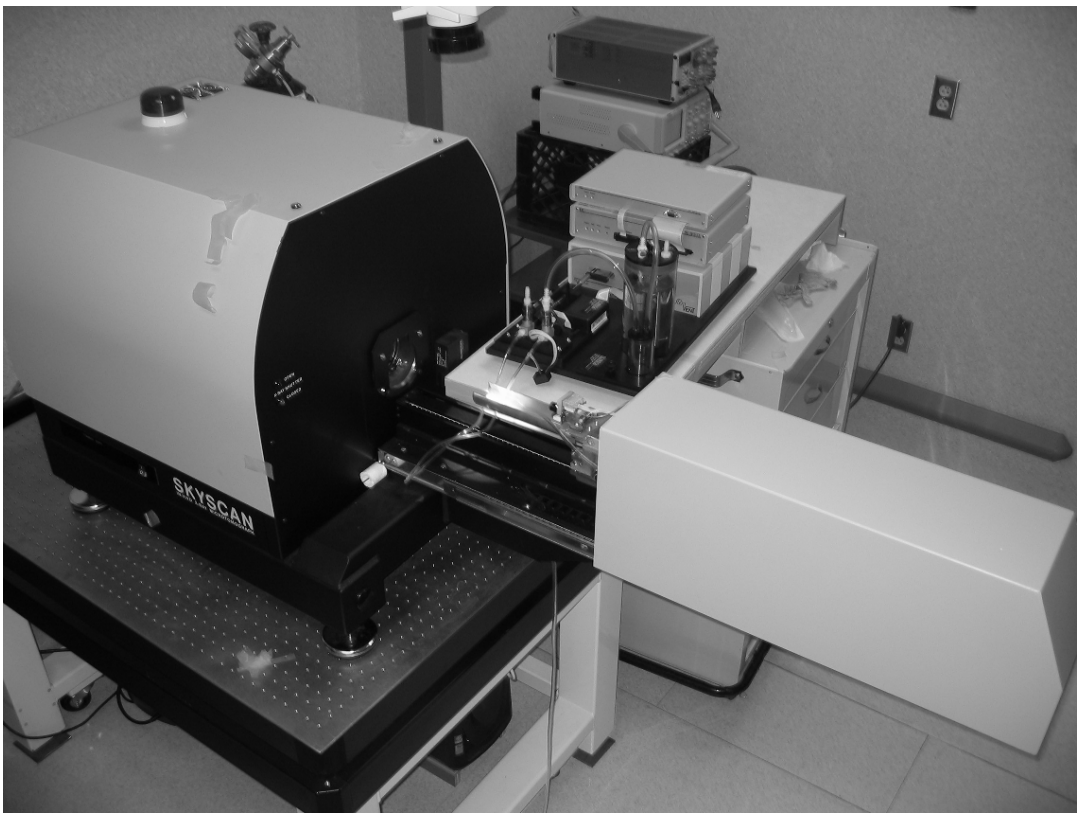

Figure 3

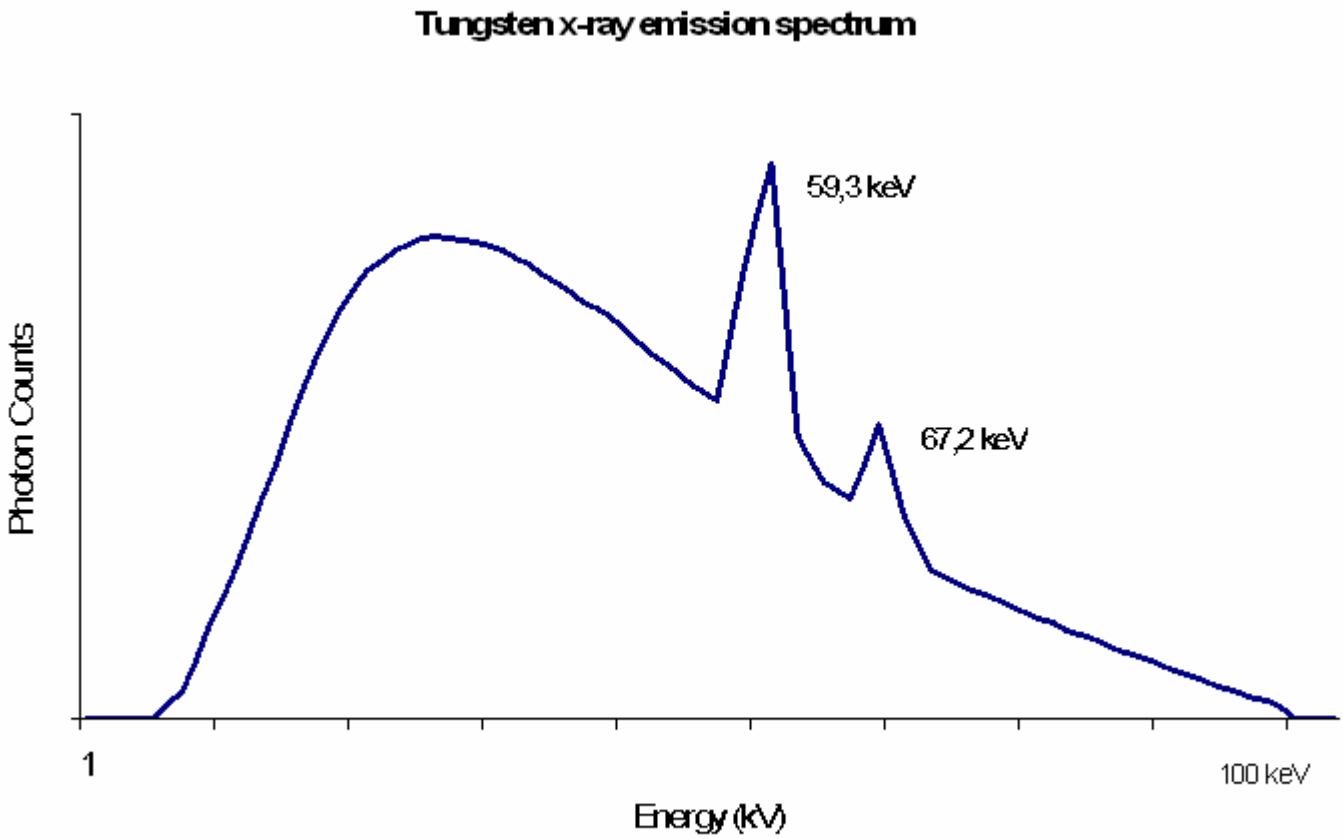
Tungsten x-ray emission spectrum
59,3 keV
67,2 keV
Photon Counts
1
100 keV
Energy (kV)

Figure 4

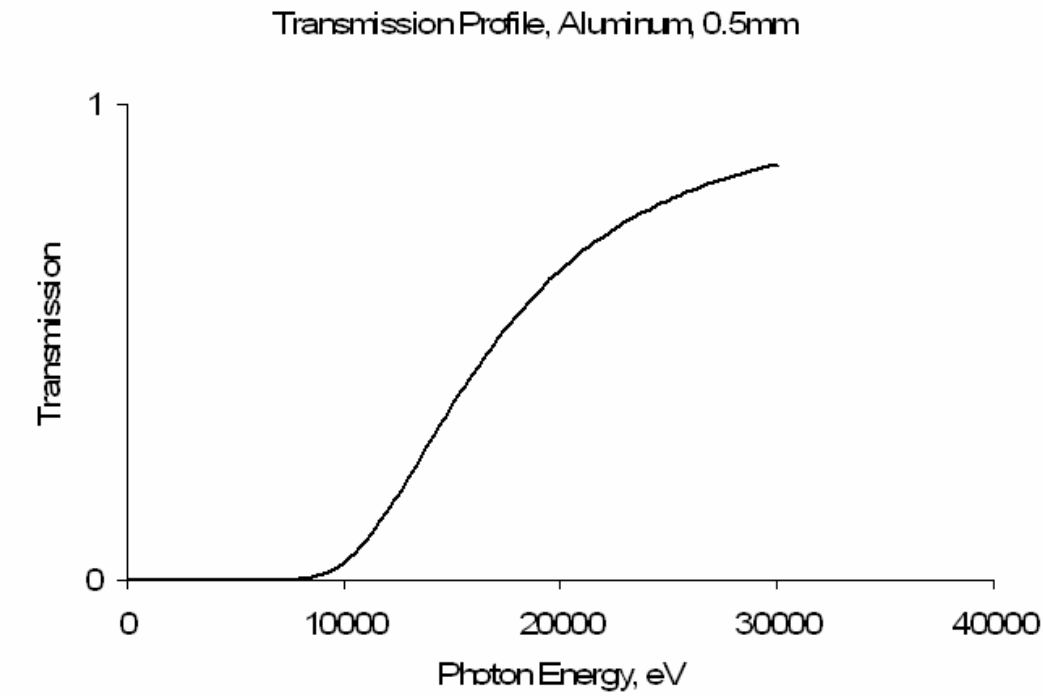
Transmission Profile, Aluminum, 0.5mm
Transmission
1
0
0
10000
20000
30000
40000
Photon Energy, eV

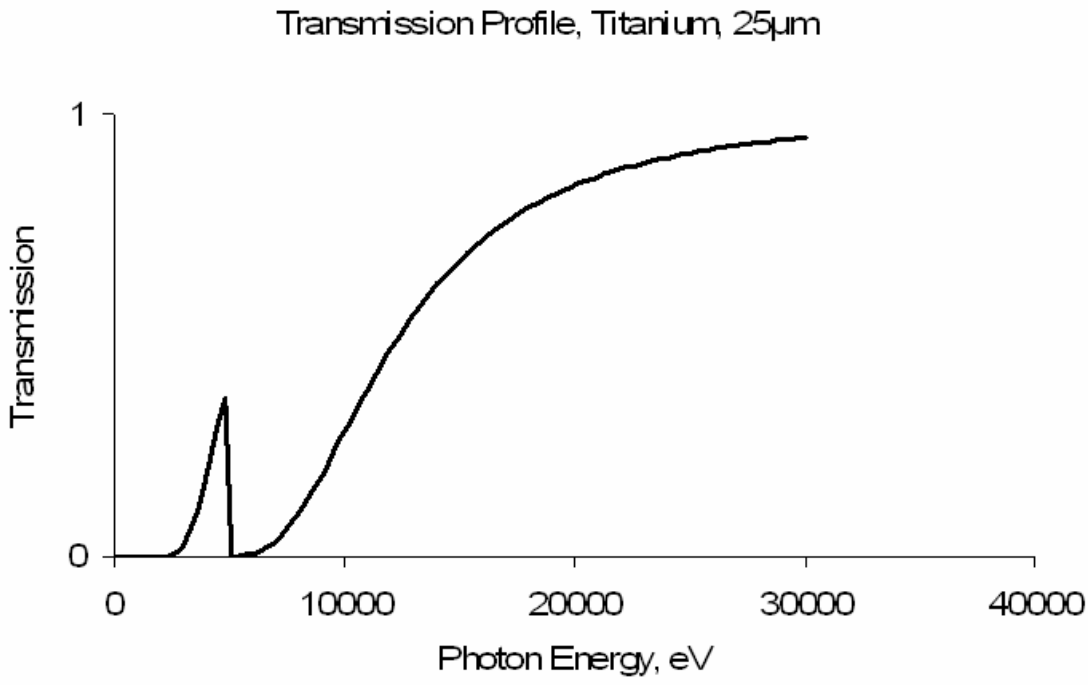
Transmission Profile, Titanium, 25µm
Transmission
1
0
0
10000
20000
30000
40000
Photon Energy, eV

Figure 5

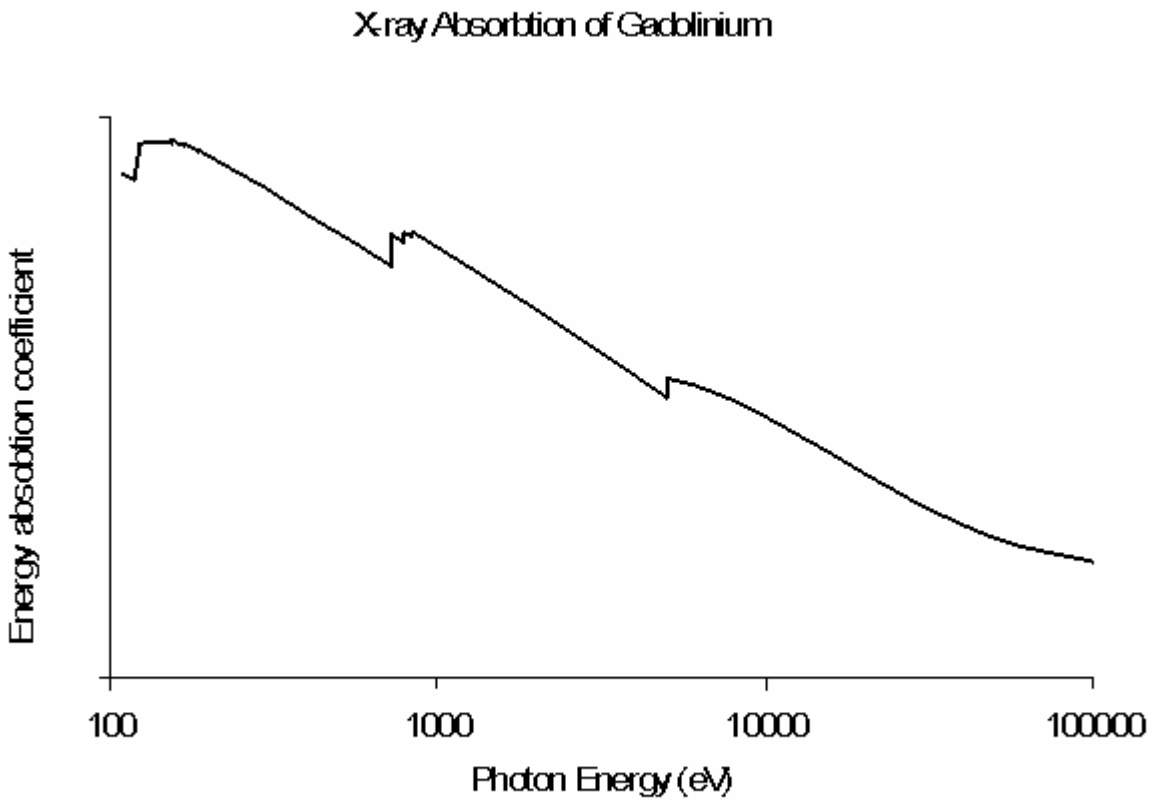
X-ray Absorbtion of Gadolinium
Energy absobtion coefficient
100
1000
10000
100000
Photon Energy (eV)

Figure 6

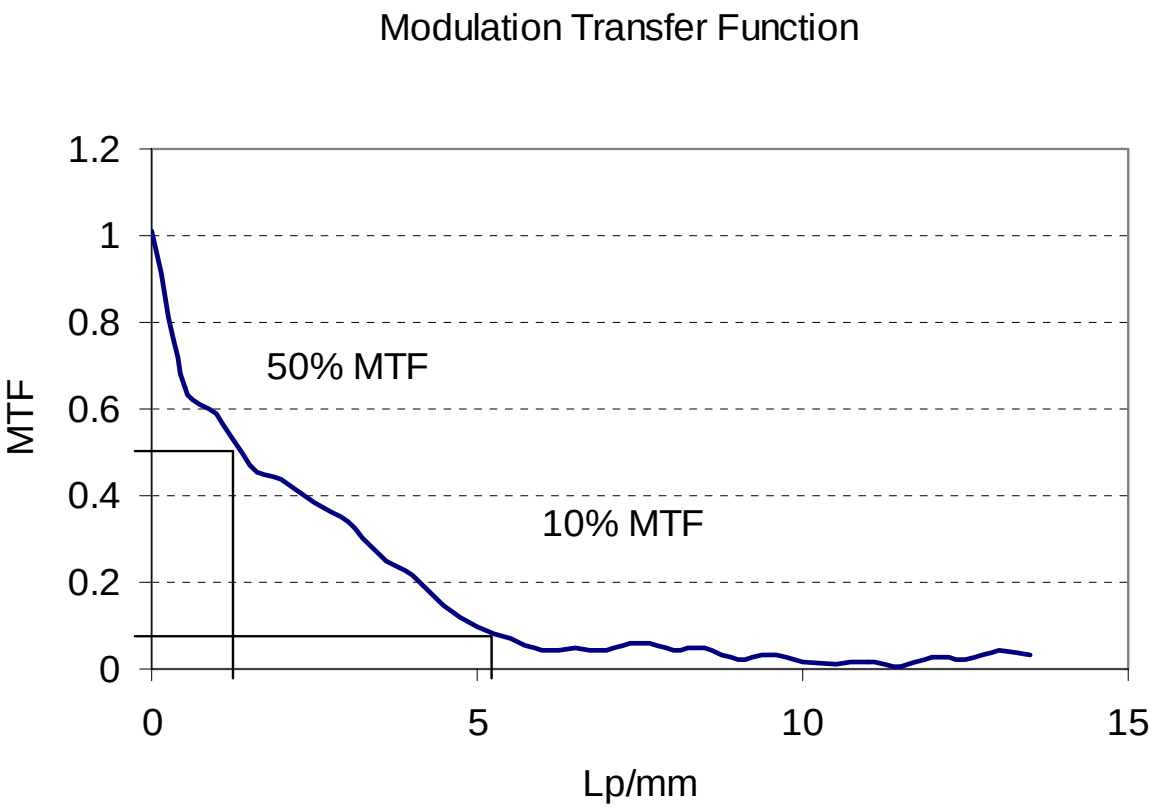
Modulation Transfer Function
1.2
1
0.8
0.6
0.4
0.2
0
MTF
50% MTF
10% MTF
0
5
10
15
Lp/mm

Figure 7

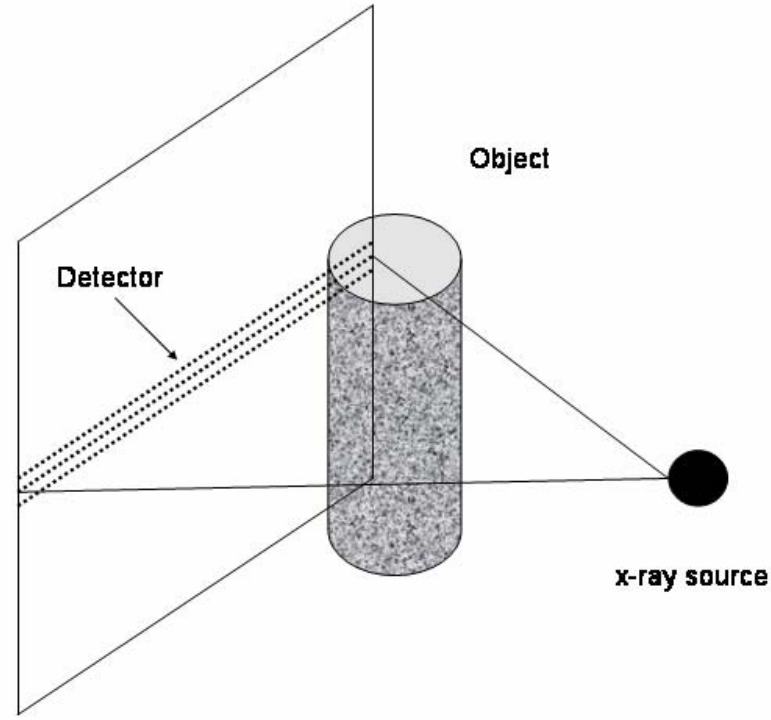

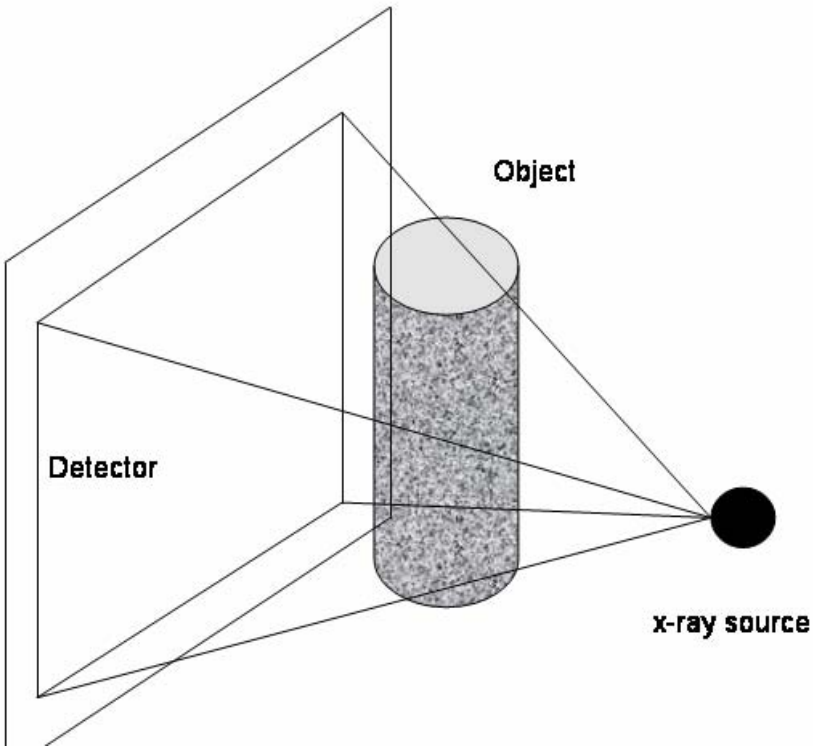

Figure 8

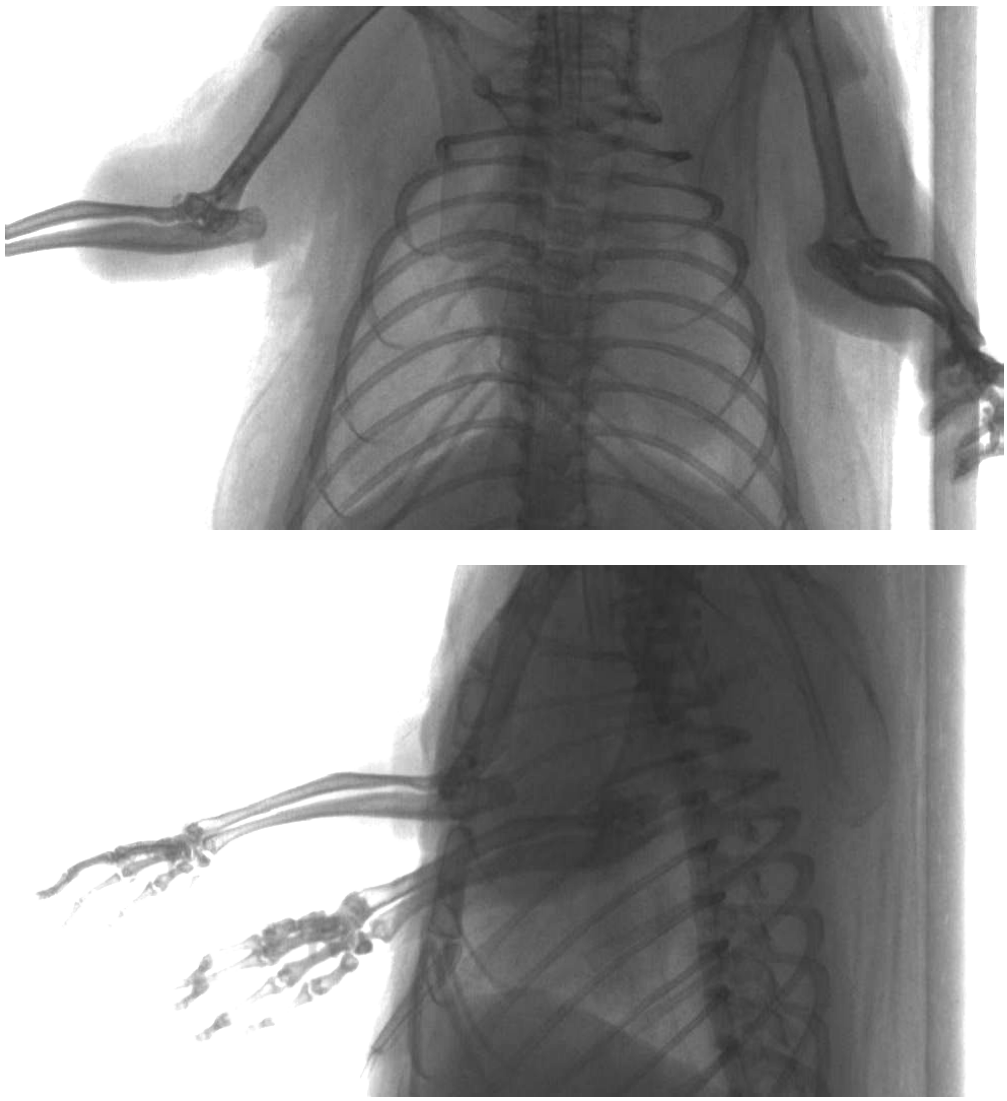

Figure 9

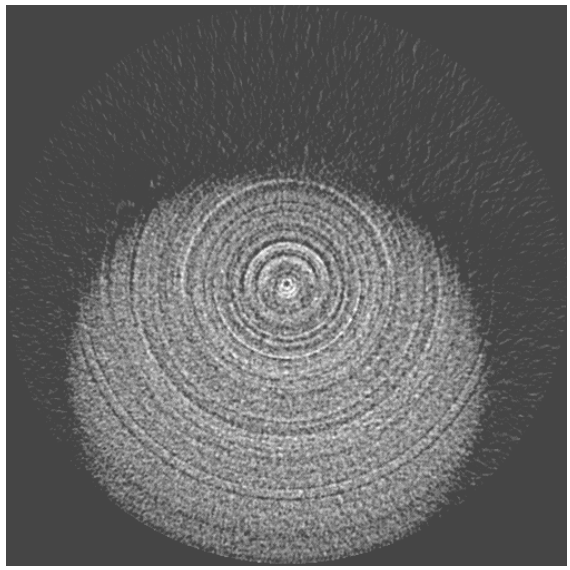

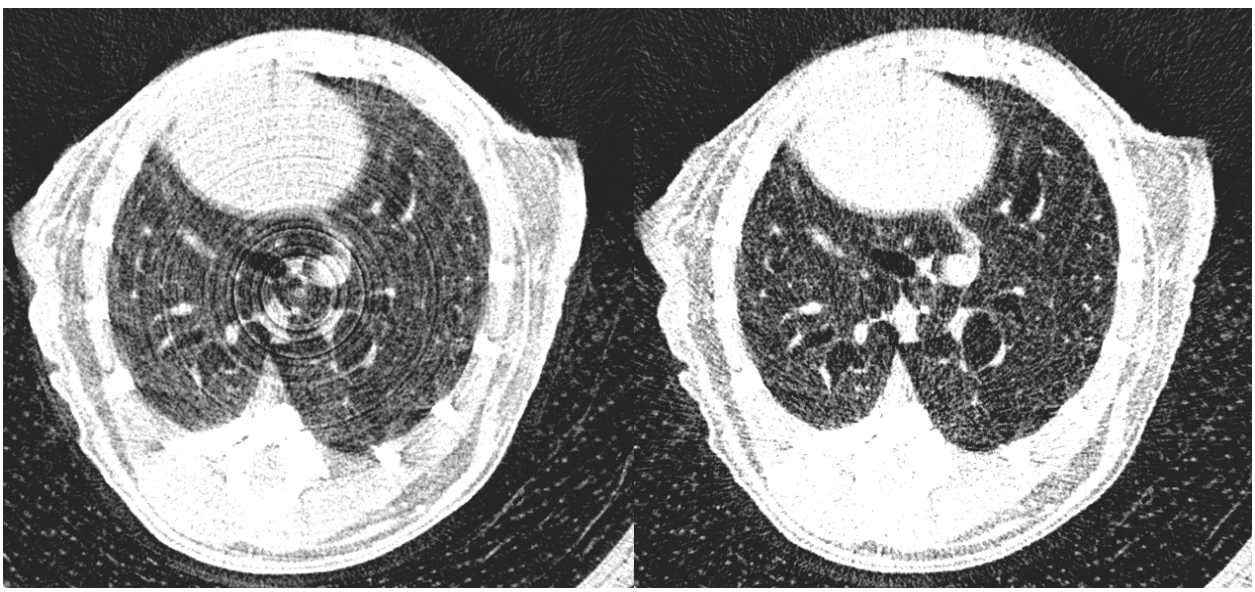

Figure 10

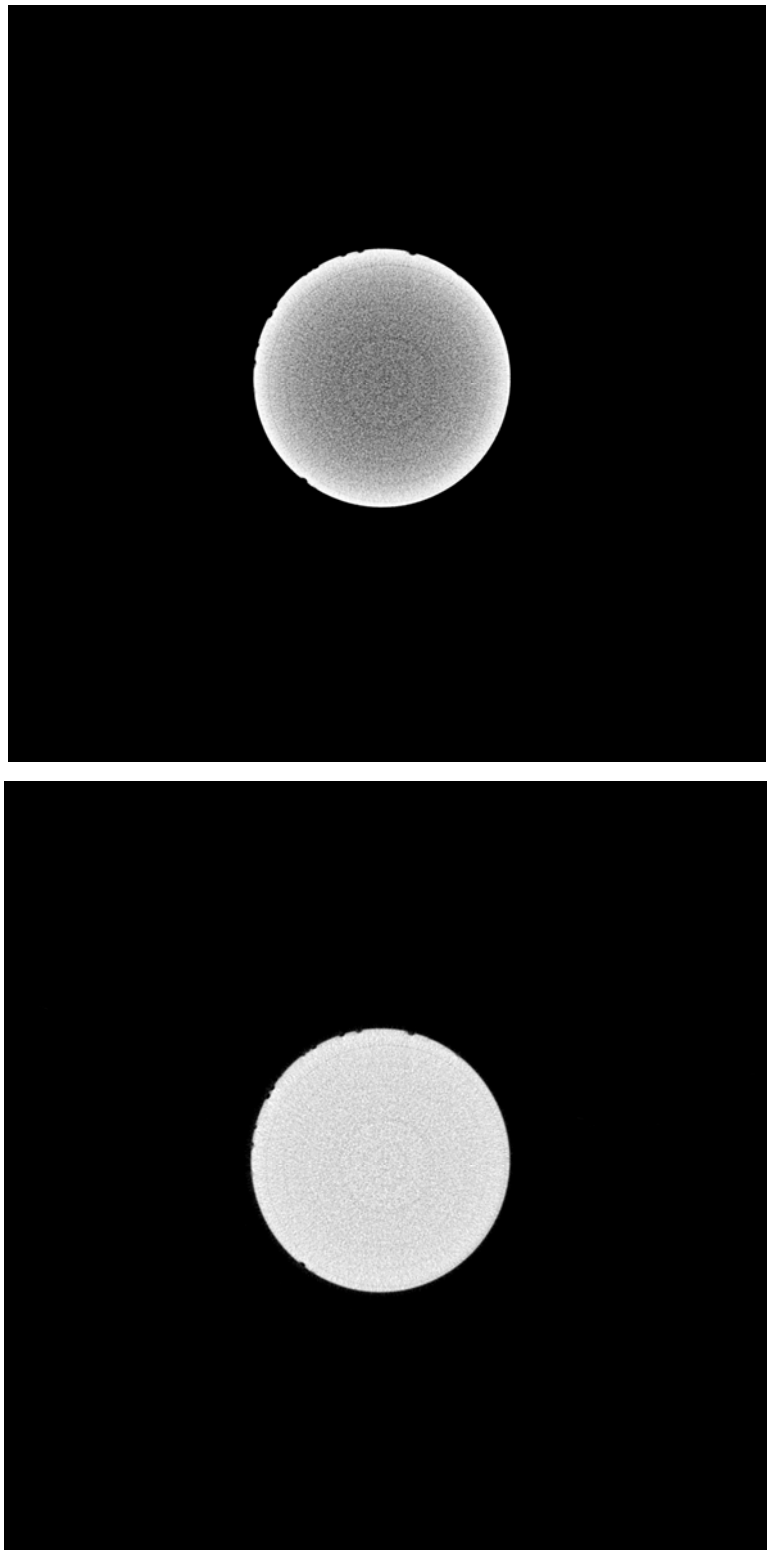

Figure 11

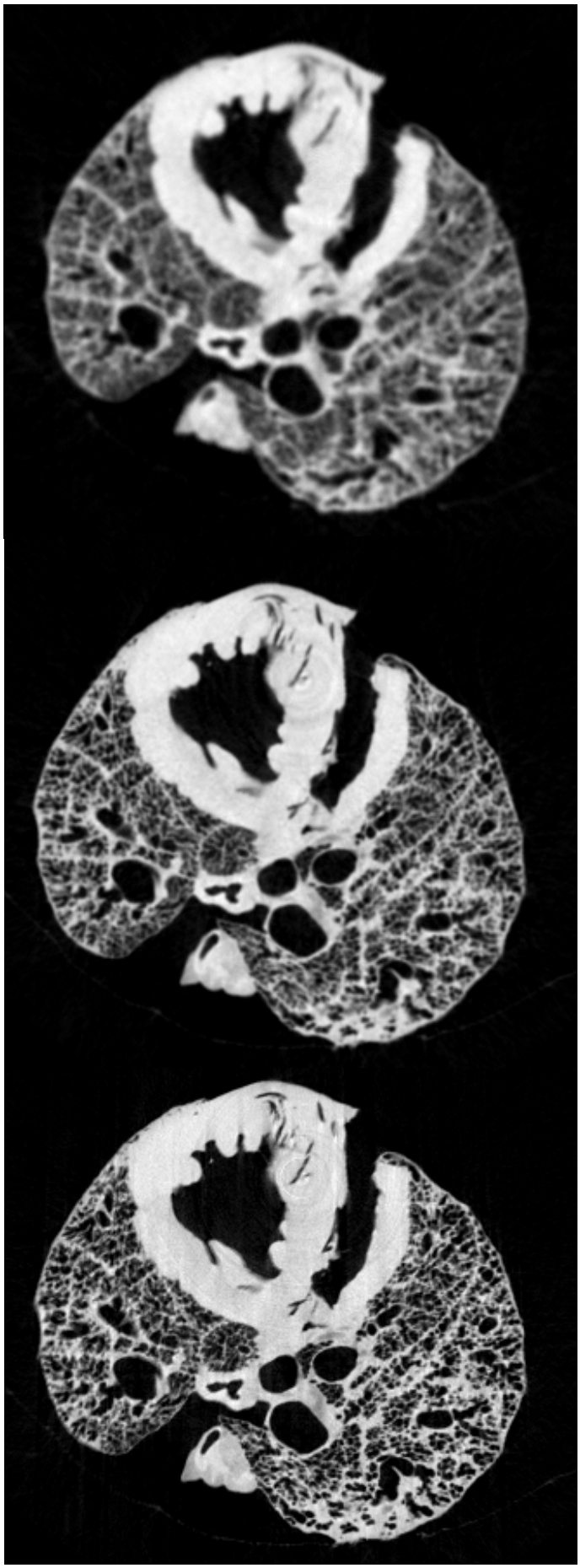

Figure 12

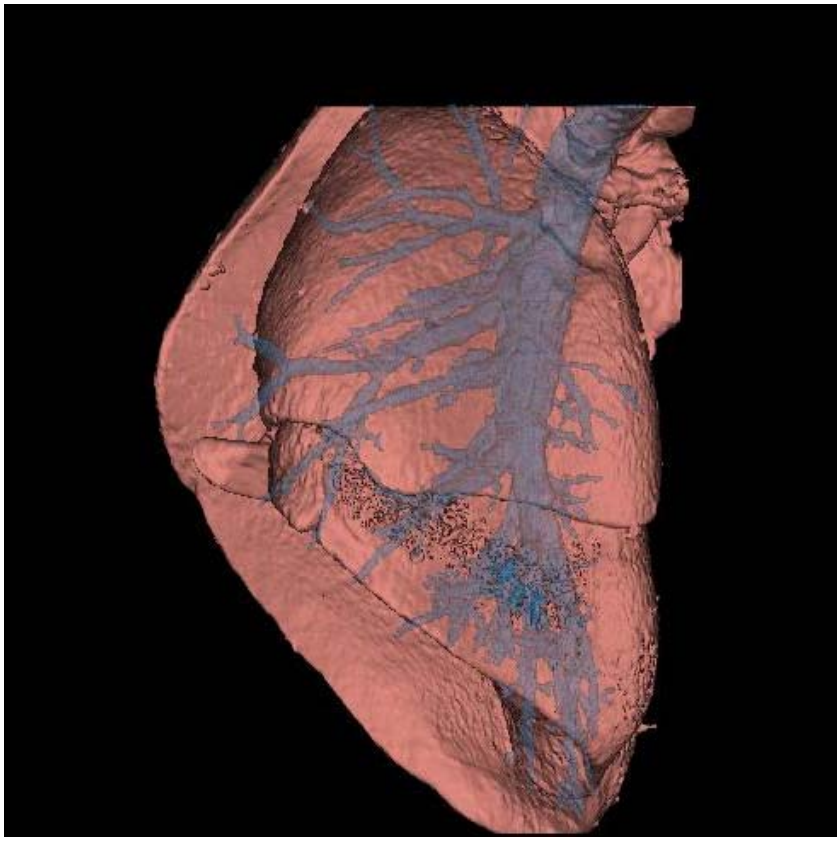

Figure 13

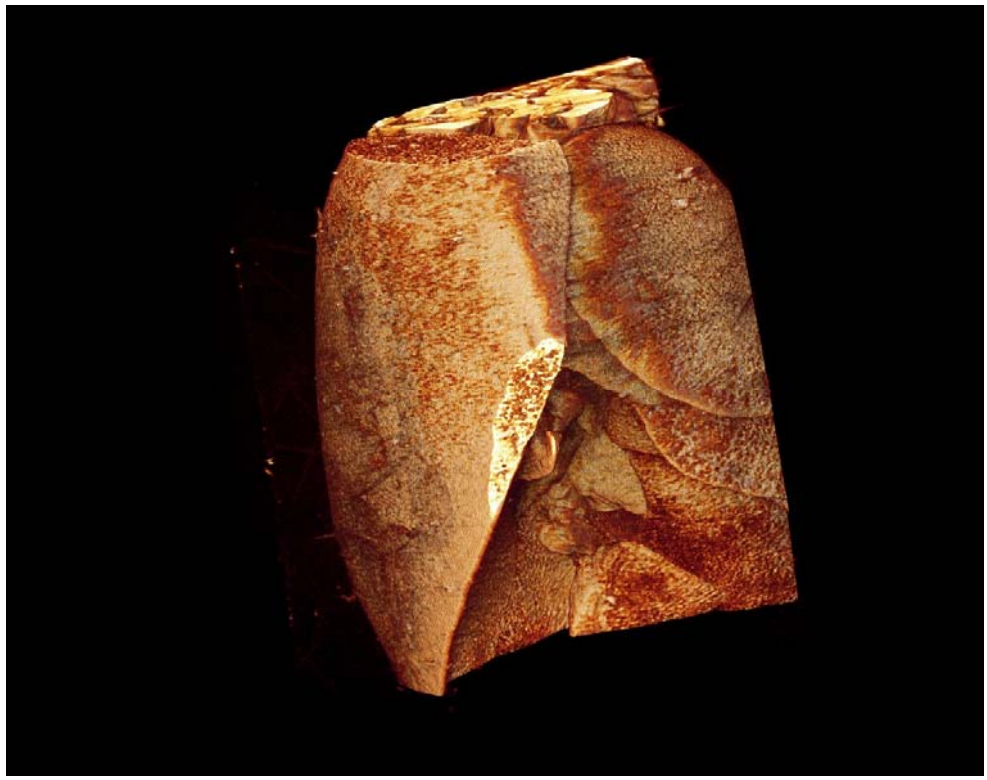

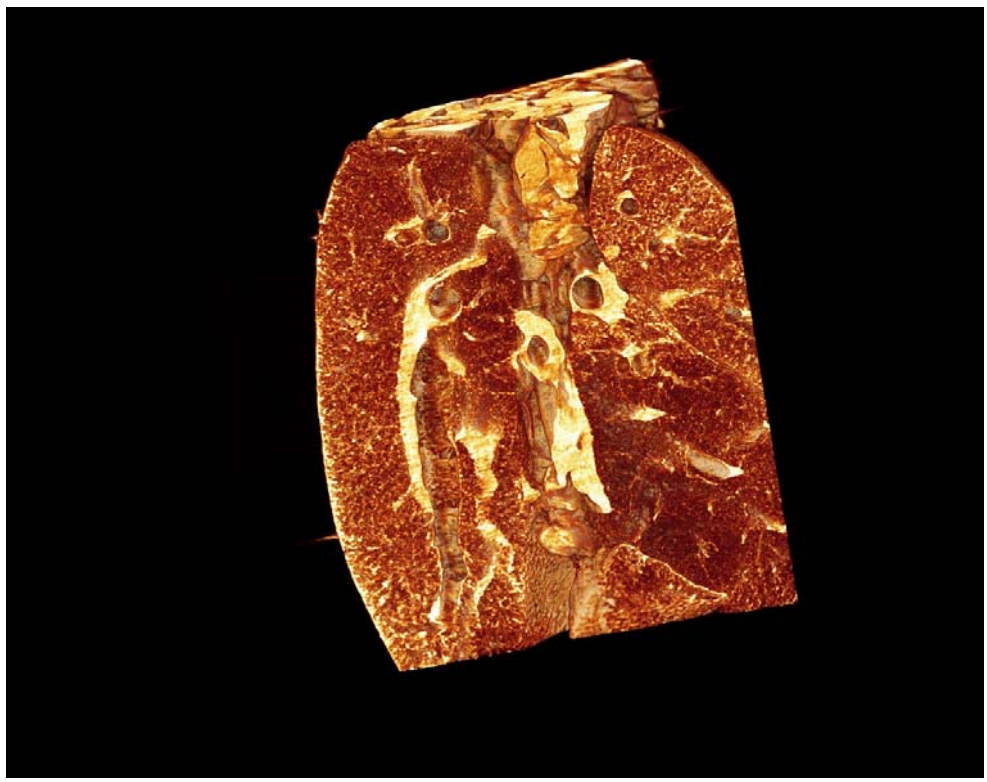

Figure 14

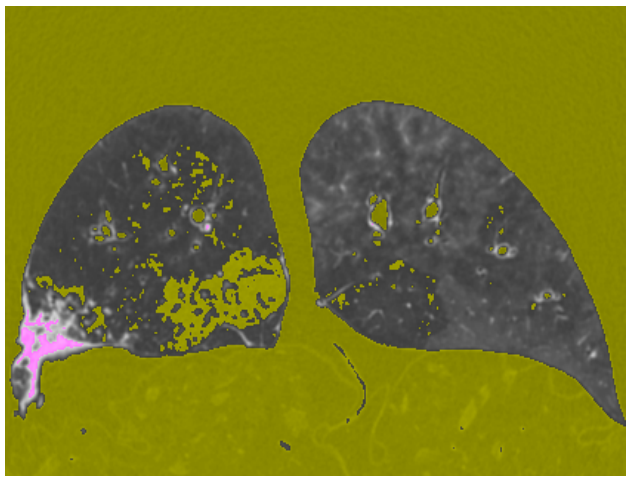

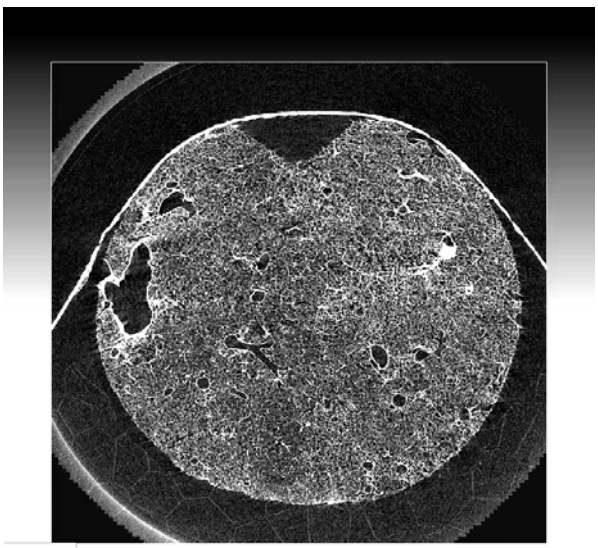

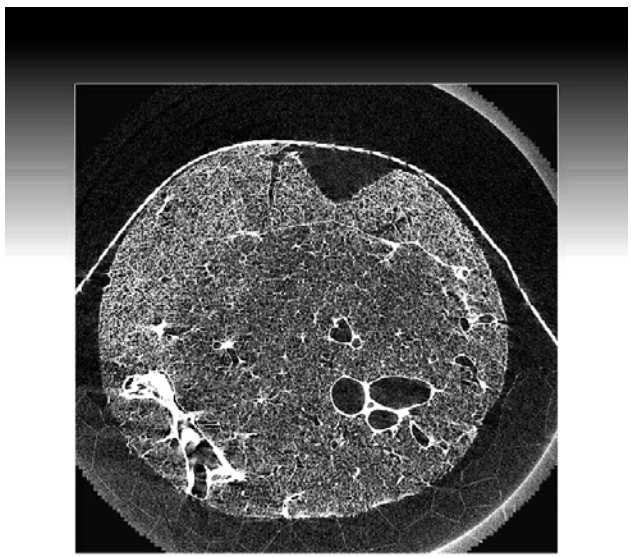

Figure 15

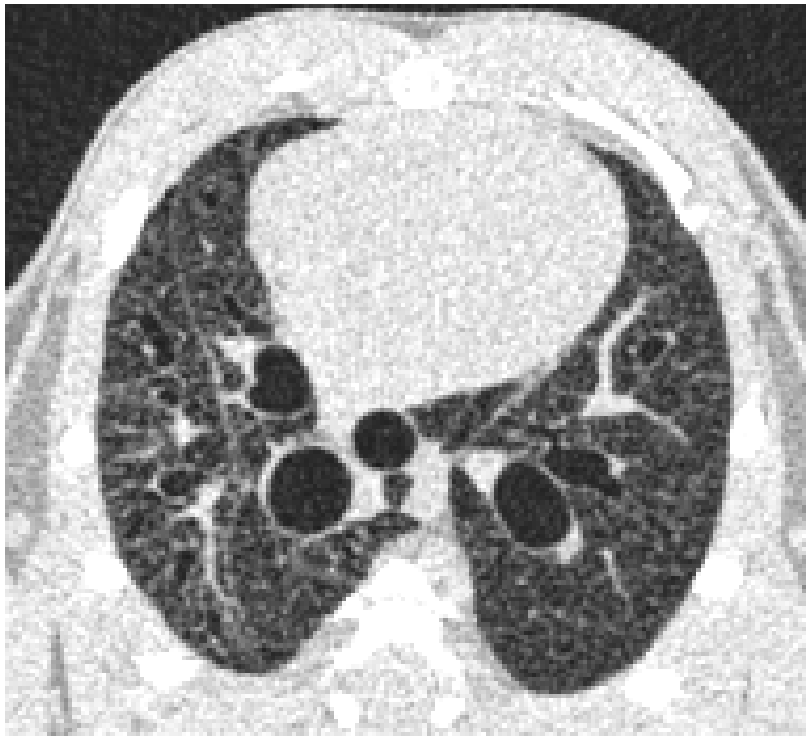

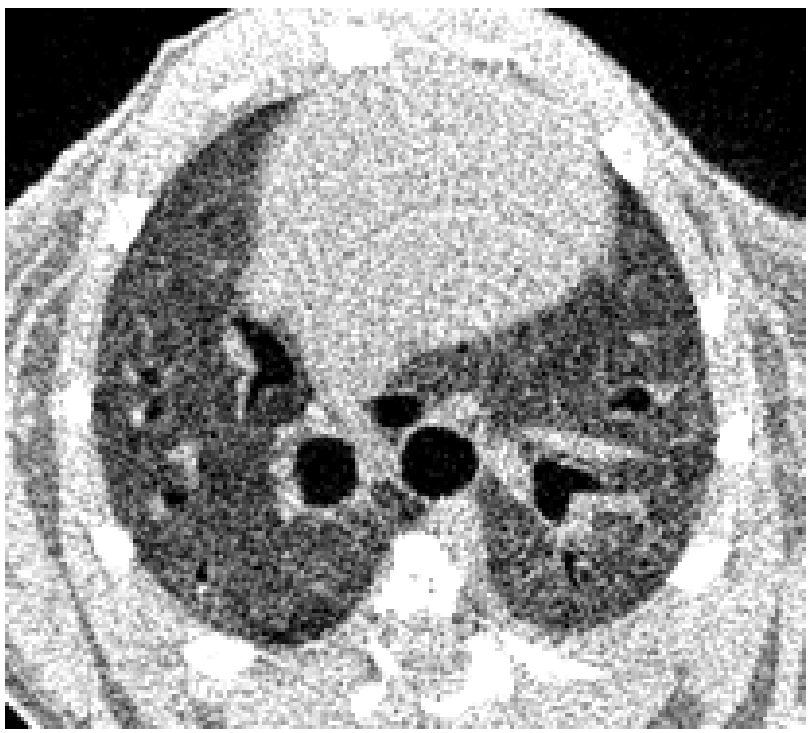

Figure 16

Figure 17

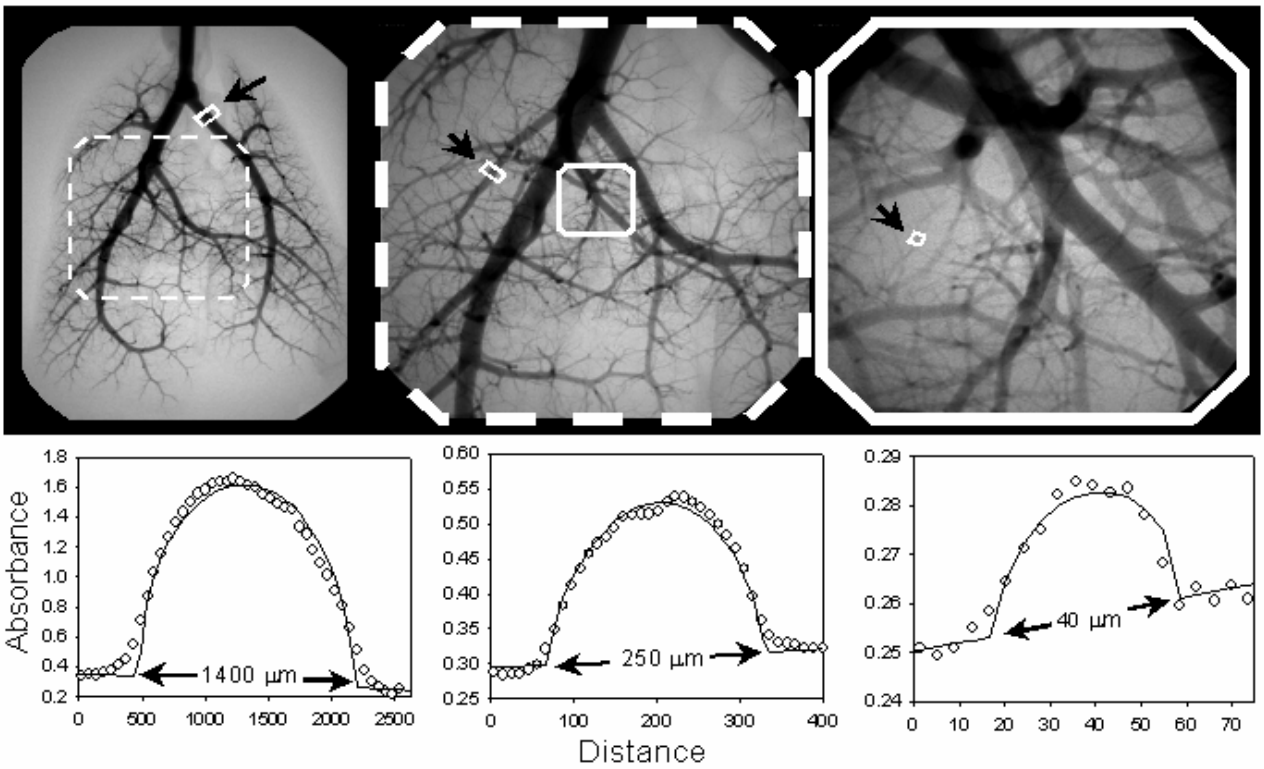

Figure 18

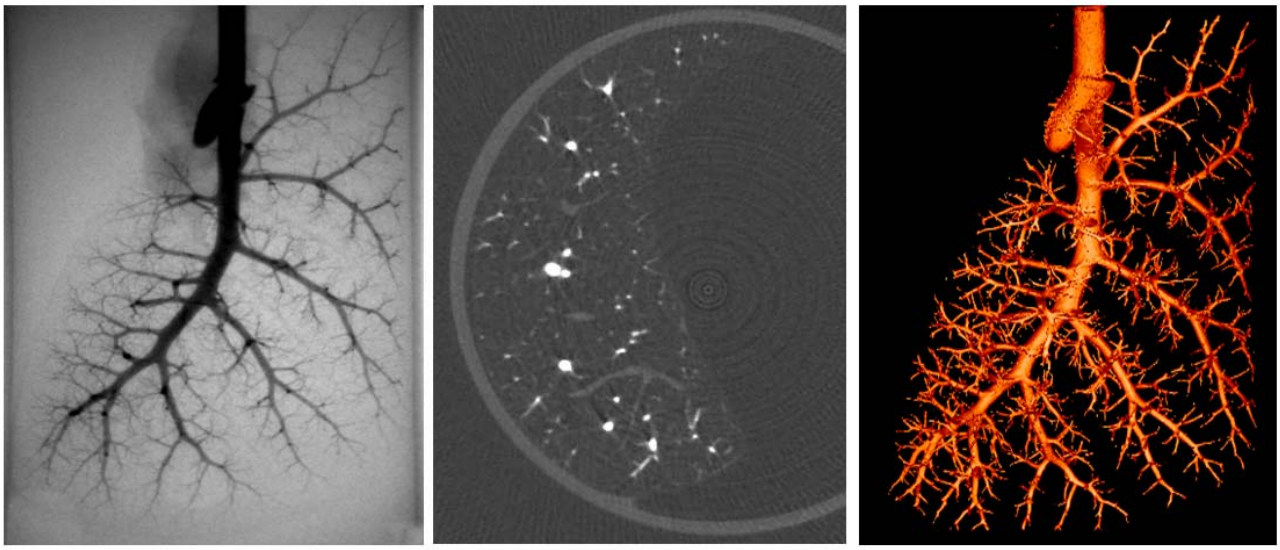

Figure 19

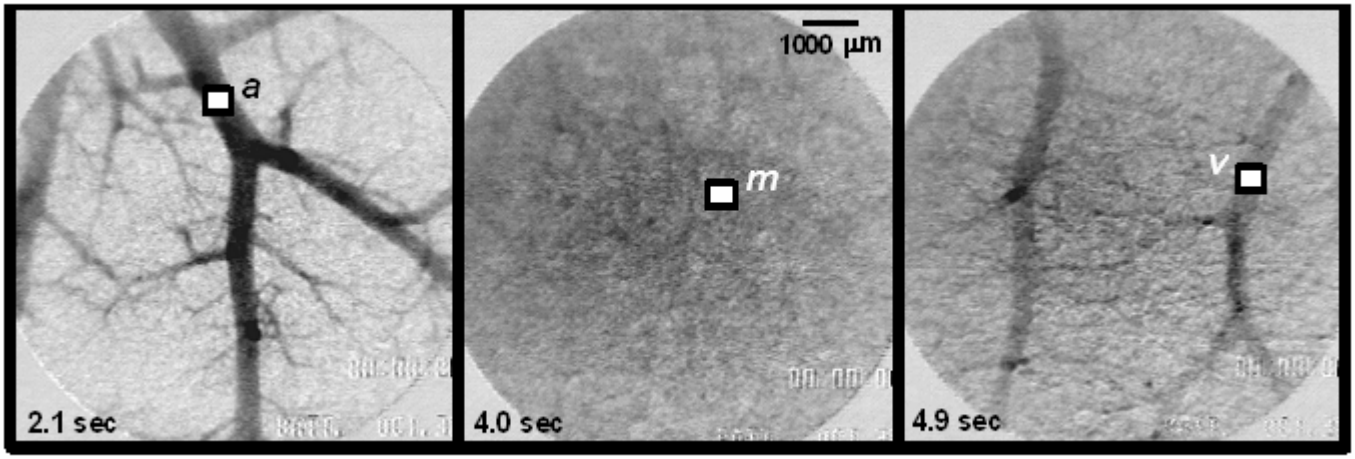
a
1000 µm
m
v
2.1 sec
4.0 sec
4.9 sec

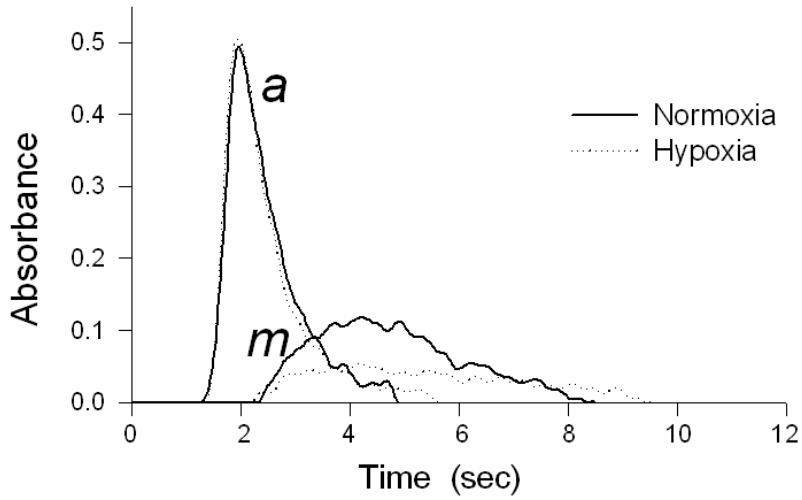
Absorbance
0.5
0.4
0.3
0.2
0.1
0.0
a
m
Normoxia
Hypoxia
0
2
4
6
8
10
12
Time (sec)

Figure 20

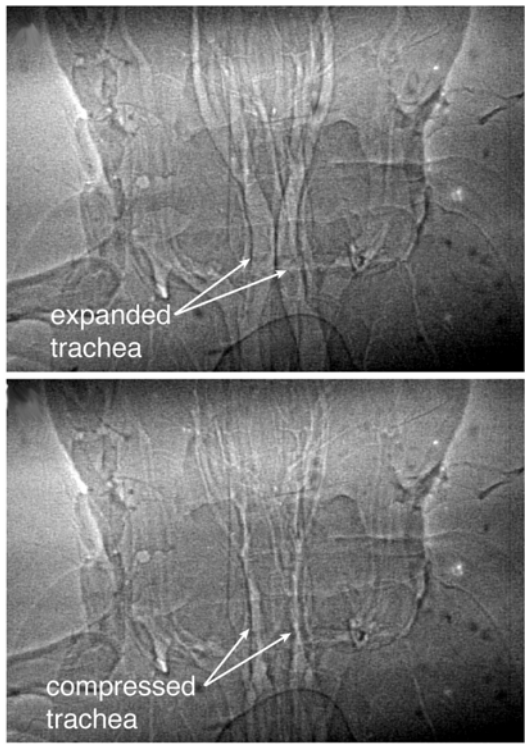

Figure 21